Available online at www.sciencedirect.com
SCIENCE DIRECT®
Coordination Chemistry Reviews 249 (2005) 1085–1110
COORDINATION CHEMISTRY REVIEWS
www.elsevier.com/locate/ccr

Review

Metal-containing molecular rectangles: synthesis and photophysical properties

P. Thanasekaran[a], Rong-Tang Liao[a], Yen-Hsiang Liu[a], T. Rajendran[a], S. Rajagopal[b,*], Kuang-Lieh Lu[a,*]

[a] *Institute of Chemistry, Academia Sinica, Academia Rd., Taipei 115, Taiwan*
[b] *School of Chemistry, Madurai Kamaraj University, Madurai 625021, India*

Received 13 May 2004; accepted 9 November 2004
Available online 5 January 2005

Contents

Abstract

This article reviews recent progress in our understanding of molecular rectangles and rectangular boxes. The synthesis of macrocycles that contain nitrogen-, oxygen-, sulphur- and phosphorus-bridged ligands is described. Synthetic routes for the preparation of the metallomacromolecules including stepwise and self-assembly strategies as well as their photophysical and molecular recognition properties are discussed. Preliminary applications of such compounds as chemical sensing devices are also briefly reviewed.

Keywords: Molecular rectangles; Molecular boxes; Self-assembly; Transition metals; Luminescence; Molecular recognition

* Corresponding authors. Tel.: +886 2 2789 8518; fax: +886 2 2783 1237.
E-mail address: lu@chem.sinica.edu.tw (K.-L. Lu).

0010-8545/$ – see front matter © 2004 Elsevier B.V. All rights reserved.
doi:10.1016/j.ccr.2004.11.006

1. Introduction

Interest in the design and construction of transition metal mediated self-assembled supramolecular entities has experienced extraordinary progress during the past decade because of their potential for use as sensors, probes, photonic devices, catalysts and in basic host–guest chemistry [1–11]. The fabrication of various lower- and higher-symmetry polygons such as triangles, squares, pentagons, hexagons, cages, and boxes has been successfully developed [12–18]. Recent reviews have focused on novel strategies for metal-mediated self-assembly in the construction of numerous metallosupramolecular squares with interesting functions [14,17]. Subsequent efforts have been devoted to the synthesis of molecular rectangles with improved selectivity and sensitivity with respect to molecular recognition and separation compared to molecular squares. Despite their relative simplicity, molecular rectangles have remained rather uncommon. In comparison with various symmetry polygons, it is difficult to assemble molecular rectangles by the simultaneous mixing of two rigid ligands of different lengths with *cis*-protected metal corners. The most important reason is that the strong enthalpic driving force favours the formation of two types of molecular squares instead of molecular rectangles [17a,c], as shown in Scheme 1.

Molecular rectangles represent a unique class of metallocycles because their preparation remains a challenge and a rectangular cavity would reasonably be expected to offer enhanced binding and selectivity. Hence, in this review article, we highlight progress in the development of molecular rectangles and discuss their photophysical properties and some preliminary applications.

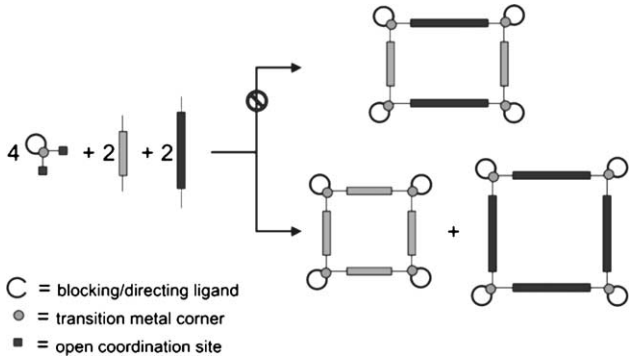

Scheme 1.

2. Molecular rectangles containing nitrogen-bridged ligands

2.1. Synthesis of Re-based molecular rectangles

The self-assembly of metal-containing rectangles from *cis*-coordinated transition metal corners and two different rigid or semi-rigid bifunctional ligands is a challenge. However, using a stepwise synthetic route, molecular rectangles can be prepared. Hupp and co-workers [19] synthesized the molecular rectangles **1** in a step-wise fashion by first creating a stable bimetallic edge using 2,2′-bipyrimidine (bpym) and then adding bifunctional pyridine based ligands (Scheme 2).

A family of molecular rectangles containing a rigid, dianionic benzimidazolate bridge has been synthesized by Hupp and co-workers [20]. Rectangle **2** offers significant advantages in overall charge neutrality, and luminescence properties. Details of the synthesis of the molecular rectangle **2** are

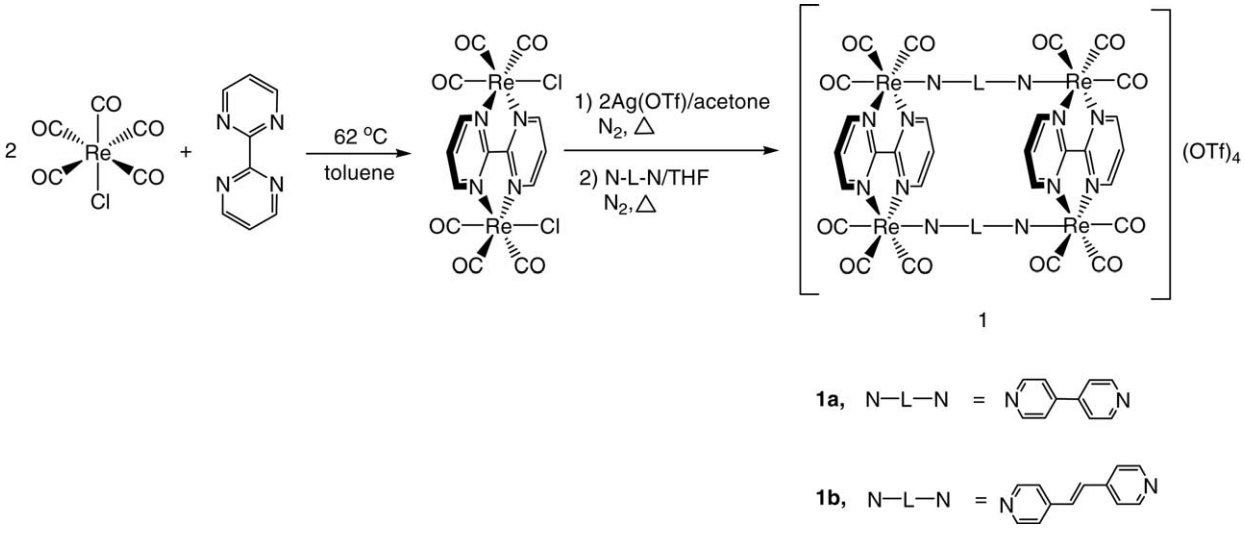

Scheme 2.

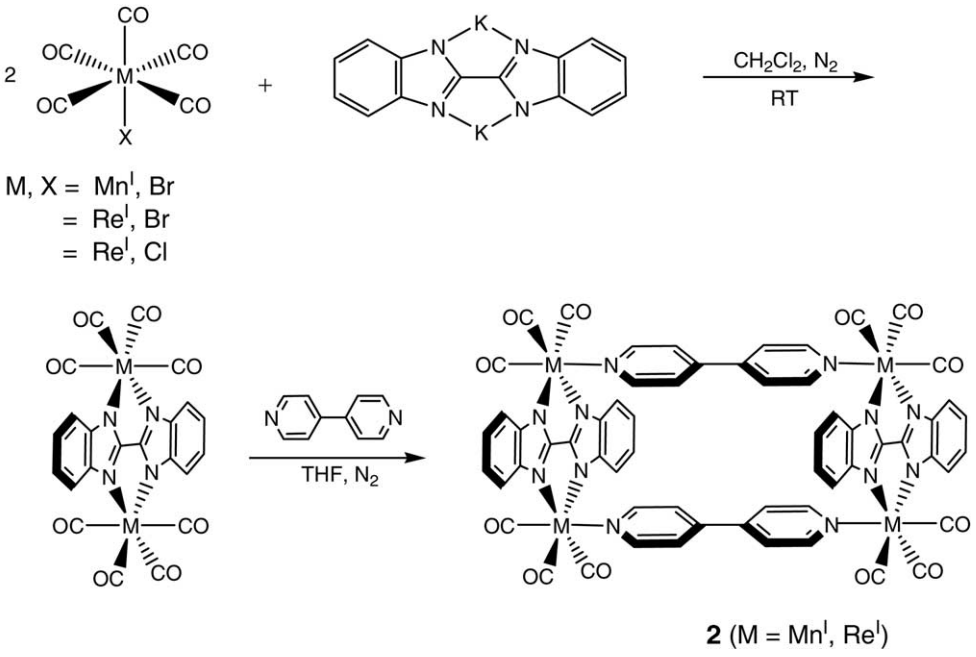

Scheme 3.

shown in Scheme 3. The solid-state packing of **2** indicates that (a) the intramolecular cavity openings of all the molecules are similarly aligned and (b) intermolecular vacancies also exist, which are effectively available for the uptake of guest molecules.

Hupp and co-workers [21] demonstrated that the reaction of bis(4-ethynylpyridyl)porphyrin with $[Re_2(CO)_6Cl_2(\mu$-bipyrimidine)] or a $[Re_2(CO)_6(\mu$-bis(benzimidazolate)) edge yields rectangles **3** and **4a**, respectively. The distance between the two porphyrins in **4a** is within 3.4 Å, slightly less than the estimated van der Waals contact distance (3.6 Å). The collapsed cavity is too narrow for the incorporation of guest molecules. However, the bent geometry of the nominally rigid ethynylpyridyl porphyrin ligand edges imparts significant charge-transfer characteristics to the rectangles. A salen-containing rectangle **4b** has also been assembled by a similar synthetic route [22].

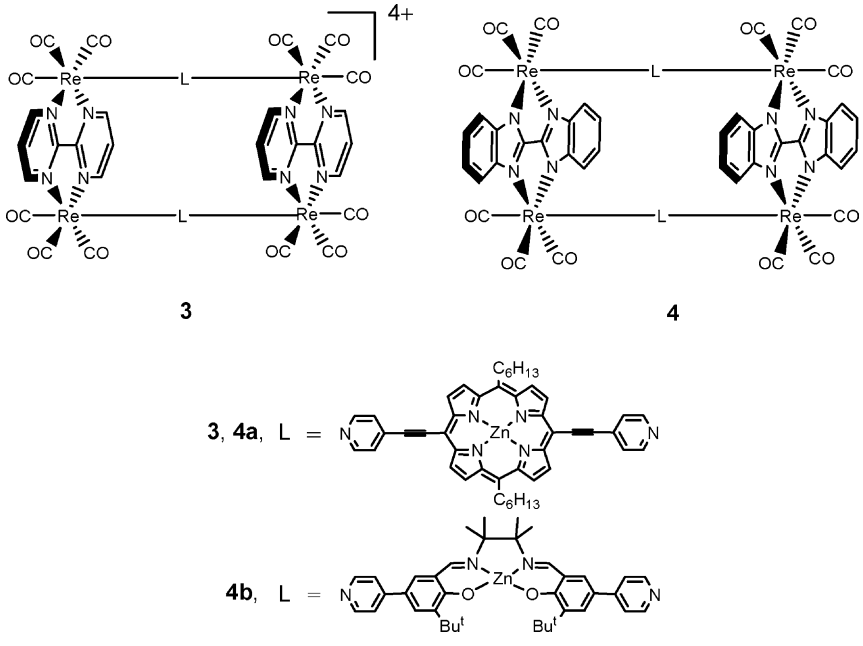

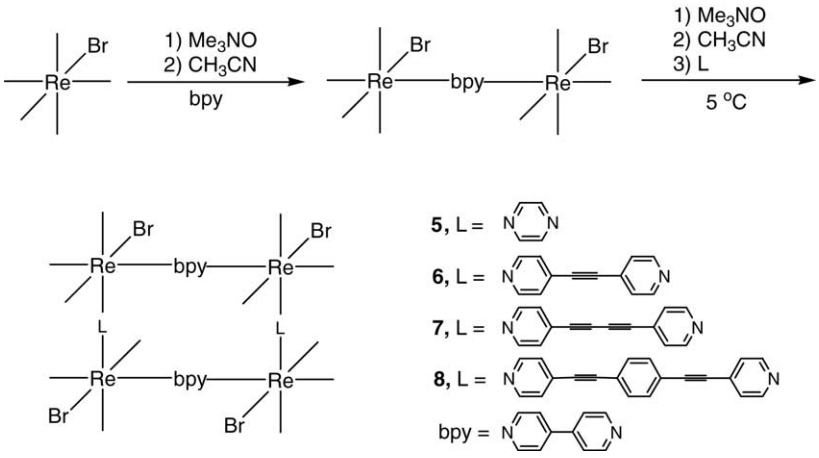

Scheme 4.

The molecular rectangles $[\{Re(CO)_3(\mu\text{-bpy})Br\}\{Re(CO)_3(\mu\text{-L})Br\}]_2$ (**5**, L = pyrazine (pz); **6**, L = 4,4′-dipyridylacetylene (dpa); **7**, L = dipyridylbutadiyne (dpb); and **8**, L = 1,4-bis(4′-pyridylethynyl)-benzene (bpeb)) have been synthesized [23a], as shown in Scheme 4. Treatment of $Re(CO)_5Br$ with Me_3NO in CH_3CN at 0 °C give $Re(CO)_4(NCMe)Br$, which on reaction with 4,4′-bipyridine (bpy), affords the $\{Re(CO)_4Br\}_2(\mu\text{-bpy})$ edge. Further treatment of the bimetallic edge with Me_3NO at 5 °C followed by the addition of pyridyl ligands affords **5**–**8**. Following a similar strategy, complexes $[\{Re(CO)_3(\mu\text{-bpe})Br\}\{Re(CO)_3(\mu\text{-L})Br\}]_2$ (bpe = *trans*-1,2-bis(4-pyridyl)ethylene); (L = pz and bpy) have also been synthesized [23b].

The solid-state packing of **5** presents an infinite number of open-end channels because of the effective π–π stacking of the aromatic rings of the molecules. The results of a molecular modelling study of **5**–**8** (Table 1) reveal that a cavity dimension of 11.4 Å × 20.8 Å could be achieved by selecting the appropriate acetylene-containing bipyridyl ligands.

Table 1
Molecular modelling data of interatomic distances (Re···Re) in **5**–**8**

Rectangle	Re–bpy–Re (Å)	Re–L–Re (Å)	L
5	11.4 (11.440)[a]	7.19 (7.214)[a]	pz
6	11.4	14.0	dpa
7	11.4	16.6	dpb
8	11.4	20.8	bpeb

Data collected from ref. [23a].
[a] From X-ray structure analysis.

With the aim of constructing molecular prisms via a self-assembly process by using the *fac*-$Re(CO)_3$ corner system, a unique class of rhenium-based, neutral, luminescent rectangular boxes were prepared [24]. Complexes $[\{(CO)_3Re(\mu_2\text{-}OR)_2Re(CO)_3\}_4(\mu_4\text{-tpeb})_2]$ (**9**, R = C_8H_{17}; **10**, R = $C_{12}H_{25}$; **11**, R = C_7H_7; tpeb = 1,2,4,5-tetraethynyl(4-pyridyl)benzene) have been obtained in excellent yields at elevated temperatures by mixing $Re_2(CO)_{10}$ and the tetradentate ligand (tpeb) in a 2:1 ratio in the alcohol of interest (Scheme 5).

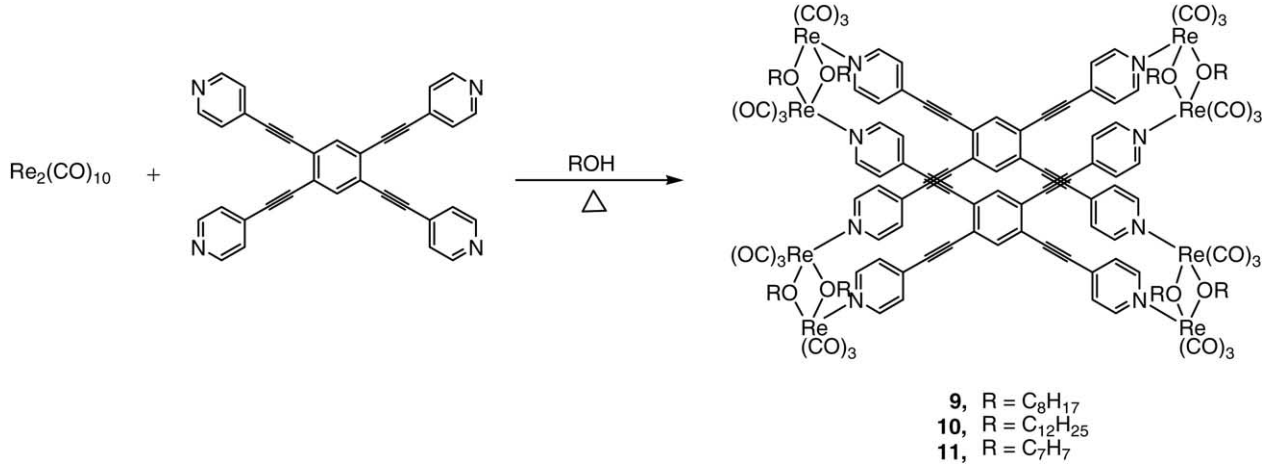

Scheme 5.

A single-crystal X-ray study of **11** revealed a rectangular box architecture with a core geometry consisting of a heavy atom prism made up of eight Re atoms. Two tpeb ligands are coordinated to four $\{(CO)_3Re(\mu_2\text{-}OCH_2C_6H_5)_2Re(CO)_3\}$ edge moieties, thereby forming a tetragonal prism.

2.1.1. Photophysics

The ground state absorption spectrum of **1** shows a solvatochromic band at 484 nm and a solvent insensitive band at 322 nm in DMSO [19]. The former band is assigned to dπ(Re) to a π^*(bpym) charge-transfer (MLCT) and the latter to an aromatic ligand localized transition. Upon excitation of **1** in CH_3CN, no detectable luminescence is observed. The parent complex $[Cl(CO)_3Re]_2$bpym] is also non-luminescent. An electrochemical investigation of **1** shows that both reduction and oxidation irreversible waves are observed for these rectangles. Based on spectroelectrochemical studies, Kaim and co-workers [25] reported a sequence of site-specific electron transfer processes to **1**.

The Re-based rectangle **2** shows an absorption band in the high energy region of the absorption spectrum and luminescence in both solution (λ_{max} = 617 in THF) and the solid state (λ_{max} = 572 nm) [20]. The lifetime of the rectangle **2** is high in the deoxygenated solvents: τ ($CHCl_3$) = 238 ns but τ (THF/MeOH) = τ (THF/MeOD) = 26 ns. The comparatively long lifetimes and substantial emission Stokes shifts suggest that the emission of **2** occurs from a predominantly triplet charge-transfer state.

The visible-region electronic absorption spectra for **3** and **4a** exhibit porphyrin-based B- and Q-bands. The Q-bands for **3** and **4a** are red-shifted by 20 and 10 nm, respectively, while comparing the Q-band for free porphyrin. This is consistent with the electron withdrawing nature of the coordinated metal. It has been experimentally shown that the cavity collapse in **3** and **4a** alters the rectangle's electronic structure and develops significant porphyrin-localized charge-transfer character to both B- and Q-band transitions. The incorporation of *fac*-$Re(CO)_3$ corners into the (salen)Zn species in **4b** results in a small change in the absorption spectrum, indicating the contribution of Re^I charge-transfer to (salen)Zn species [22]. On excitation of their MLCT band, the emission maximum is also red-shifted from 677 to 694 nm for **3** and to 704 nm for **4a** in comparison to the free porphyrin. Both **3** and the free porphyrin have the same emission lifetime, 1.3 ns with an emission too weak for a reliable measurement of **4a**. In **4b**, the (salen)Zn moiety is fluorescent at room temperature in solution and electronic energy transfer occurs within the salen assemblies. Cyclic voltammetry studies of **3** and **4a** in THF show reversible reduction potentials. For free porphyrin: −0.96 and −1.39 V; for **3**: −0.70, −0.95, −1.06, −1.18 V; and for **4a**: −0.89, −1.08, and −1.20 V versus Ag/AgCl. All are assigned as porphyrin reductions, except the first and fourth reductions for **3**. The relatively good reduction waves accessible to the coordinated bipyrimidine edges suggest redox quenching and may account for the attenuation of the fluorescence of **3**.

Table 2
Absorption and emission spectral and excited state lifetime data for **5**–**8** in CH_2Cl_2 at 298 K

Compound	Absorption λ_{max} (nm)	Emission λ_{max} (nm)	Lifetime τ (ns)
5	252, 336	606	86
6	259, 352	611	86
7	259, 323, 357	616	72
8	260, 351	616	495

Data collected from ref. [23a].

Table 2 summarizes the spectral absorption data of **5**–**8**. The electronic absorption spectra of **5**–**8** [23] exhibits two absorption bands in the near-UV region. The bands, which appear at higher energy, are assigned to a ligand centred π–π^* transition and the lower one to a metal-to-ligand charge-transfer (MLCT) transition. These results are consistent with previous reports [3a,5].

The maxima of emission spectra (λ_{max}^{em}) and the excited-state lifetime (τ) of **5**–**8** are summarized in Table 2. The broad luminescence spectra of **5**–**8** indicates that the luminescence originates solely from the lowest ^{3}MLCT state. The assignment of the lowest emitting level as MLCT in character is supported by the position and shape of the emission band and the emission lifetime, which is consistent with previously reported data [26–28]. Though the emission lifetimes of **5**–**7** are similar, it is very high for **8**. The probable explanation for this is that the ^{3}MLCT state of **8** is suitably positioned such that it is away from ^{3}MC as well as from the ground state. A possible alternative explanation for the long lifetime of **8** compared to **5**–**7** is the involvement of the extended π system of the bpeb ligand.

Cyclic voltammetric data for **5**–**8** in CH_2Cl_2 show two reduction waves and three oxidation waves. The first reduction wave at around −1.0 V versus SCE is assigned to the reduction of the non-bpy ligand, and the second reduction to the bpy ligand. The first oxidation of **5**–**8** around 0.4 V may be assigned to oxidation of the bromide ion [29]. The quasireversible oxidation waves observed in the range 1.35–1.70 V versus SCE may be attributed to the oxidation of the metal centres present in the rectangle. This redox behaviour of these rectangles can be exploited in their utilization as electron donors in the efficient electron transfer reactions with electron acceptors and electron donors [30].

The UV–vis spectra of **9**–**11** shows a sharp absorption near 318 nm and a shoulder at 363 nm in THF [24]. The sharp intense absorption at 318 nm is consistent with the π–π^* transition of the highly conjugated bridging ligand tpeb, and the shoulder at 363 nm to the MLCT transition (Re → tpeb). Although, the emission could not be detected at RT, **9**–**11** are emissive at 77 K and photophysical data are given in Table 3.

The rectangular boxes **9** and **11** are weakly emissive at room temperature when pyridine is used as the solvent. The emission maxima are at 636 nm for **9** and at 641 nm for **10**; an emission spectrum could not be obtained for **11**, since it is insoluble in pyridine. The emission lifetimes of **9** and **10**

Table 3
Spectral and photophysical data of **9**–**11**

Box[a]	Absorption λ_{max} (nm)	Emission λ_{max} (nm)	Quantum yield (Φ) $\times 10^{-4}$	Lifetime (τ) ns	Emission (77 K)[b] λ_{max} (nm)
9	208, 321, 369 (sh)	655	2.88	52	628
10	208, 320, 357 (sh)	645	9.77	66	624
11	208, 321, 360 (sh)	667	1.40	26	624

Data collected from ref. [24].
[a] For **9** and **10**, 20% THF–80% H_2O and for **11**, 20% DMF–80% H_2O were used.
[b] For **9** and **10**, THF and for **11**, DMF were used as solvents.

in pyridine at room temperature are 22 and 37 ns, respectively. To improve the luminescence properties of **9**–**11**, the emission spectra in organic solvent–water mixtures were recorded, and the results are presented in Table 3. Interestingly, a significant improvement is observed in the emission intensity of **9**–**11** in 80% H_2O–20% organic solvent mixture. The enhanced emission in the presence of water might be due to the formation of self-aggregates.

2.1.2. Molecular recognition

In order to understand the binding ability of rectangle **1**, 2,6-naphthelenedisulfonate was selected as a guest molecule [19]. The binding ability of **1** was monitored by following the change in the chemical shift of protons by ^{1}H NMR and the reported binding constant value is close to $2.3 \times 10^3\ M^{-1}$. In addition to a van der Waals component, Coulombic interactions favour host–guest interactions.

The emission of the Re-based rectangle **2** is rapidly and dynamically quenched by various electron donors at diffusion-controlled rates, rather than by binding interactions [20]. Quantitative assessments of the host behavior of **2** toward selected volatile organic compounds (VOCs) as guests were obtained by quartz crystal microgravimetry measurements and the binding affinities are given in Table 4. At a high concentration of guest molecules, the guest–host stoichiometry exceeds unity with a hypothetical limiting ratio between 1:1 and 2:1. Electron withdrawing substituents diminish the affinity constant, whereas electron-donating substituents enhance it. These results suggest a significant role for host–guest interactions, including guest uptake.

Since the cavity of **3** and **4a** [21] possesses the flexible nature of porphyrin moiety, experiments were carried out to examine the binding of guests to these rectangles. A strong Lewis base, DABCO (1,4-diazobicyclo[2.2.2]octane) was observed to bind to **4a** with a binding constant $5 \times 10^4\ M^{-1}$, whereas quinuclidine was found to bind to **4a** with $K_B = 2 \times 10^5\ M^{-1}$, suggesting that these guests are binding to the exterior of **4a**.

Table 4
Binding affinities of thin film of Mn-based rectangle **2** and a representative "molecular square" towards selected VOCs

VOC	Mn-based **2** [M^{-1}]	[Re(CO)$_3$Cl(η-pz)]$_4$ [M^{-1}]
Toluene	3200 ± 1900	332 ± 26
4-Fluorotoluene	1400 ± 360	200 ± 42
Benzene	740 ± 250[a]	157 ± 8
Fluorobenzene	420 ± 80	87 ± 8
Hexafluorobenzene	460 ± 110	47 ± 8

Data collected from ref. [20].
[a] Value for Re-based rectangle **2** is $580 \pm 220\ M^{-1}$.

Since Re-based rectangles **5**–**8** possess a large cavity and are luminescent in nature [23], redox quenching reactions of **5**–**8** with several organic electron acceptors and electron donors were studied. Interestingly, these substrates efficiently quench the luminescence of **5**–**8**, with quenching rate constants (k_q) in the range 3.0×10^7–$6.2 \times 10^{11}\ M^{-1}\ s^{-1}$. The decrease in the emission intensity of **7** with an increase in the concentration of the quencher (1,2-chloranil) is shown in Fig. 1. Although, the Stern-Volmer plots drawn from the luminescence intensity and lifetime data are linear, intensity quenching is more efficient than lifetime quenching implying the contribution of static quenching [31,32]. The association constants for the binding of 1,4-naphthaquinone with **6**–**8** are 280, 295, and $1202\ M^{-1}$, respectively, and for 9,10-anthraquinone with **6** and **8** are 124 and $178\ M^{-1}$, respectively.

To investigate the binding capabilities of **9**–**11** [24], the absorption and emission spectra of pyrene in the absence and presence of **9**–**11** were recorded. Interestingly, an increase in the absorbance of pyrene due to complex formation is observed with increasing concentrations of **9**–**11**. Based on absorption spectral measurements, a linear Benesi–Hildebrand plot indicates 1:1 complex formation between **9**–**11** and pyrene, and the binding constants were found to be in the range 2.2×10^4 to $9.2 \times 10^4\ M^{-1}$. Efficient quenching of the emission from the pyrene was also noted with increasing concentrations of **9**–**11**. The Stern-Volmer plot is linear at low concentrations giving quenching rate constants of 2.1×10^{13} to $2.6 \times 10^{13}\ M^{-1}\ s^{-1}$; but at higher concentrations, a deviation from linearity is observed. This behaviour indicates that quenching occurs after the binding of pyrene to **9**–**11**. A further ^{1}H NMR study of **9** with increasing concentrations of pyrene revealed an upfield shift in the signals, corresponding to the pyridyl and phenyl hydrogens of the tpeb ligand, when 0.08 M pyrene was used. In contrast, the chemical shifts of the alkoxy protons were unaffected upon the addition of pyrene. These observations suggest that pyrene is recognised as a guest molecule by the tpeb ligand of **9**–**11**.

2.2. Synthesis of Pt- and Pd-based molecular rectangles

Stang and co-workers [33] reported the synthesis of nanoscopic metallacyclic rectangles **12**–**15** from the reac-

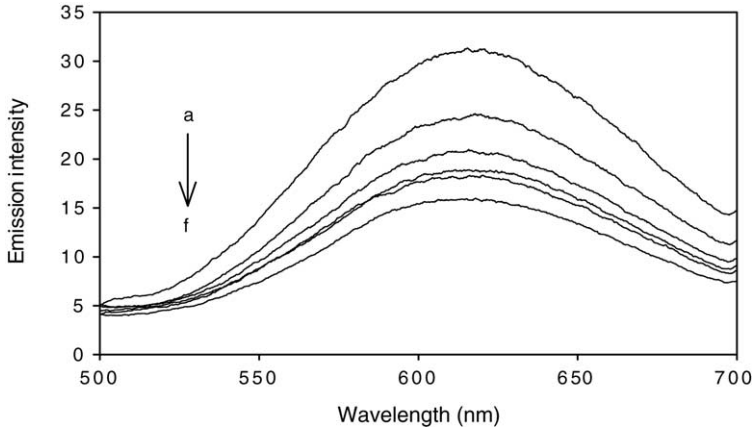

Fig. 1. The emission intensity of rectangle **7** (8×10^{-5} M) decreases with increasing quencher (1,2-chloranil) concentrations of (a) 0 M, (b) 2×10^{-4} M, (c) 3×10^{-4} M, (d) 4×10^{-4} M, (e) 5×10^{-4} M, and (f) 6×10^{-4} M in CH_2Cl_2. Reprinted with permission from ref. [23a]. © 2003 American Chemical Society.

tion of a predesigned Pt-based molecular clip, 1,8-bis(*trans*-$Pt(PEt)_3)_2(NO_3)$anthracene, with rigid dipyridyl bridging ligands, in 92–97% yields via spontaneous self-assembly (Scheme 6). The assembly of these macrocycles was monitored by ^{1}H NMR and ^{31}P {H} NMR spectrometry. Spectroelectrochemical studies of **12** and **13** [34] indicate reduction at the neutral acceptor ligands, and oxidation at the dianionic Pt-based anthracene clips.

Building upon a similar strategy, another example of a Pt-based rectangle has recently been described by Stang and co-workers [35]. A functionalized ligand, 3,8-bis-pyridin-4-ylethynyl-[1,10]-phenanthroline, undergoes self-assembly

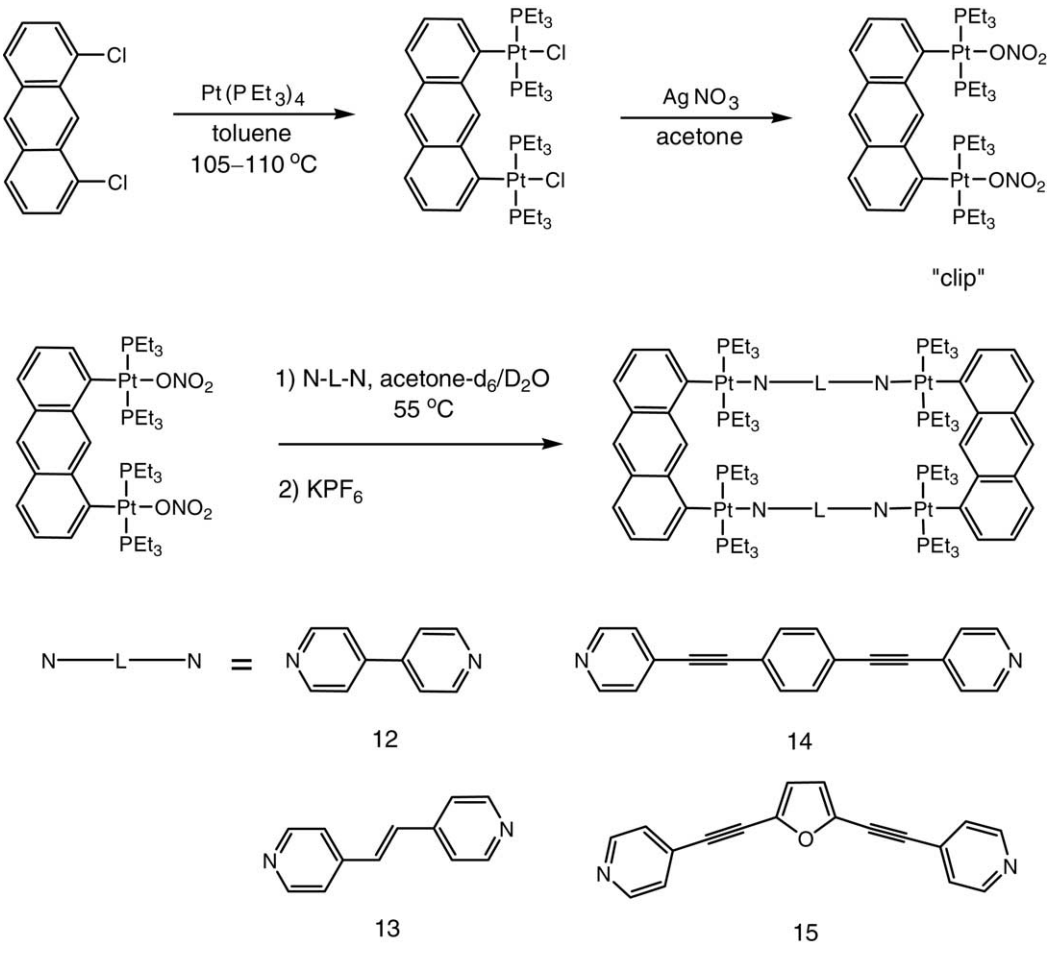

Scheme 6.

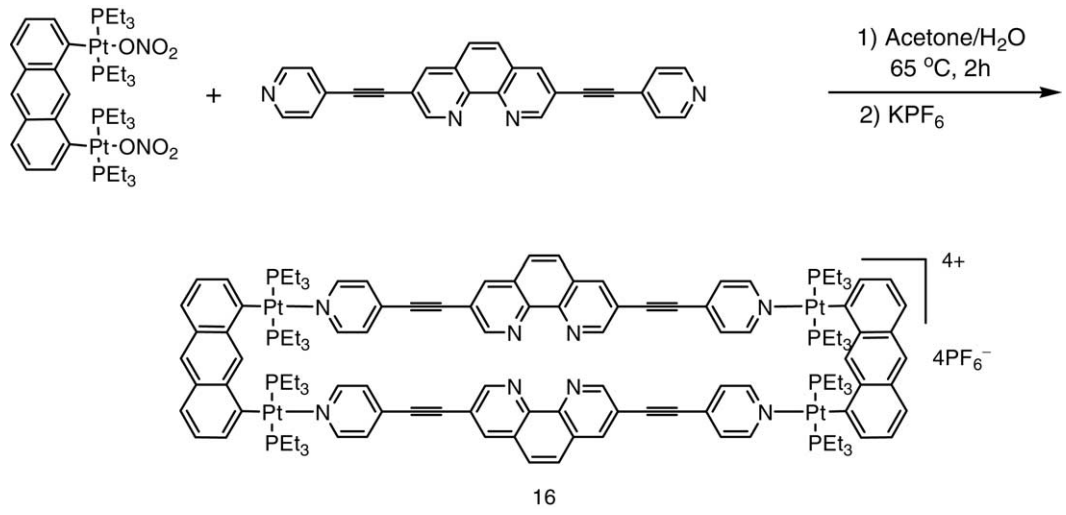

16

Scheme 7.

with a Pt-based anthracene clip to form the functional molecular rectangle **16** (Scheme 7).

Lippert and co-workers [36] prepared Pt-based rectangles **17** and **18** by two different routes. By mixing the mononuclear bis(purine) complex, *trans*-[$(NH_3)_2$Pt(9-MeA-*N*7)(9-MeGH-*N*7)]$(NO_3)_2\cdot H_2O$ with an excess of *trans*-a_2PtCl_2 (a = NH_2CH_3 or NH_3), dinuclear complexes were formed. In the dinuclear platinum complexes, the Pt–N(1) and Pt–N(7) vectors are approximately orthogonal, therefore making these complexes potential building blocks for the formation of molecular rectangles. As a result, the diplatinated A–G base pair, upon loss of HCl, could undergo a condensation reaction to form the closed rectangle **17**. Alternatively, a trinuclear platinum complex was first prepared by the reaction of *trans*-$[(NH_2CH_3)_2Pt(H_2O)_2]^{2+}$ with two equivalents of *trans*-[$(NH_3)_2$Pt(9-MeA-*N*7)(9-MeGH-*N*7)]$(NO_3)_2\cdot H_2O$ at pH 4–5. The triplatinated A–G base pair then reacts with one equivalent of *trans*-$[(NH_2CH_3)_2Pt(H_2O)_2]^{2+}$ to afford **18**. ^{1}H NMR spectra recorded in DMSO-d_6 and DMF-d_7 provide evidence for a head–head arrangement of the two N(7)-bound purine bases, while A–H2 and G–N(1)H resonances are split in a 4:1 ratio, indicative of the presence of two rotamers in these solvents.

Lippert and co-workers [37] were able to synthesize hexanuclear Pt_2Pd_4 species **19** by the reaction of *trans*-$[a_2Pt(Hampy)_2](NO_3)_2$ (a = $MeNH_2$; Hampy = 2-aminopyridine) with an excess of $[(en)Pd(H_2O)_2{}^{2+}]$ (en = ethylenediamine) in an aqueous solution. The $(en)Pd^{II}$ moiety in **19** exclusively bridges the amido groups of four ampy ligands in such a way that an open rectangular box is formed.

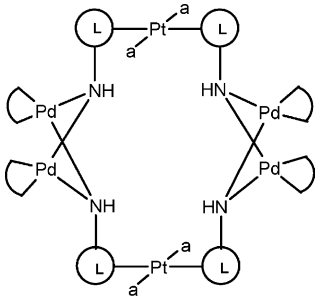

19, a = $MeNH_2$, L = 2-aminopyridine

An interesting example of a redox-active Pd-based rectangle $[(\eta^5\text{-}C_5H_4C_2\text{-}3\text{-}py)_2Fe]_2Pd_2Cl_4$ (**20**) prepared from $PdCl_2$(COD) [38] and the $(\eta^5\text{-}C_5H_4C_2\text{-}py)_2Fe$ moiety

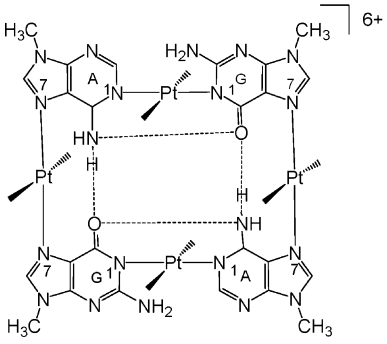

17

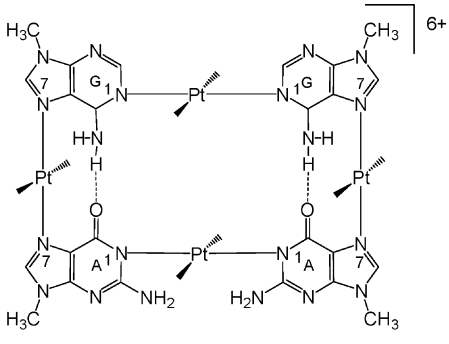

18

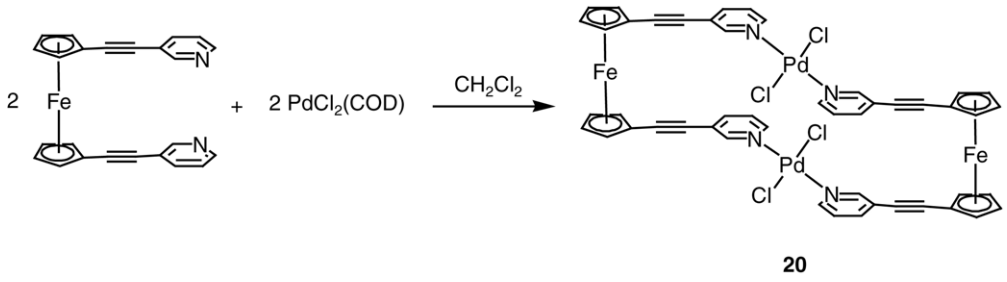

20

Scheme 8.

(Scheme 8) was reported by Lindner et al. [39]. The IR spectra show that the absorption for the C=N and C≡C stretching vibrations is shifted to higher wave numbers relative to the free ligands. This is consistent with the coordination of transition metals to nitrogen. The low solubility of **20** in solvents precludes any studies of its electrochemical behavior.

The nanoscale molecular rectangle **22** using the molecular clip **21** with palladium and linear linkers such as 4,4′-bipyridine has been constructed by Bosnich and co-workers [40] (Scheme 9). The ^{1}H NMR spectrum of **22** is highly symmetrical. Both the spacer-chelators and 4,4′-bipyridine groups of **22** have identical chemical shifts, consistent with a D_{2h} point group on the NMR time scale.

2.2.1. Photophysics

The electronic spectrum of **13** exhibits near UV-transitions, which are red-shifted relative to BPE (*trans*-1,2-bis(4-pyridyl)ethylene) (π–π^*) and slightly blue-shifted relative to the molecular clip starting material [33]. The extinction coefficient per BPE unit increases upon the formation of a rectangle, while the absorbance of the anthracene moiety, centred at 270 nm, decreases. This can be attributed to the electronic reorganization of the conjugated, aromatic framework. Although, anthracenes have been widely applied as luminescent tags, no emission is detected for **13** due to the contribution of a heavy atom effect.

The UV–vis spectrum of **16** in methanol shows several absorption bands at 350, 280 and 230 nm [35]. These bands are diagnostic of changes in the electronic structure of the macromolecule.

2.2.2. Molecular recognition

The addition of Ni(II)$(NO_3)_2{\cdot}6H_2O$ to a solution of **16** [35] in methanol induces a dramatic change in the UV–vis

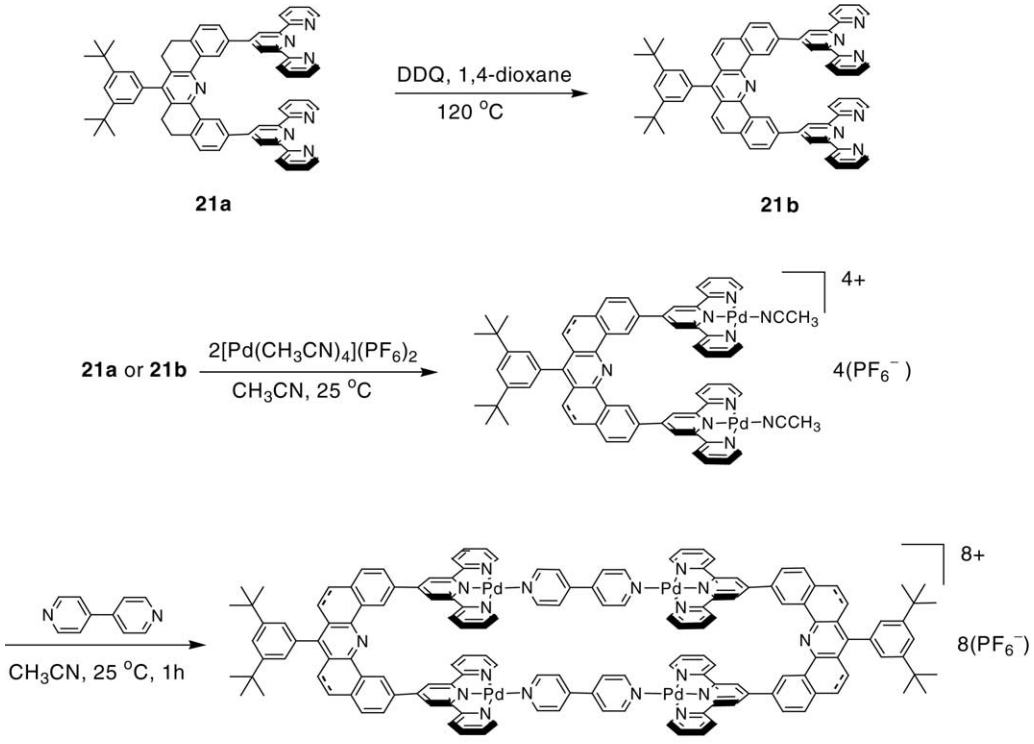

22

Scheme 9.

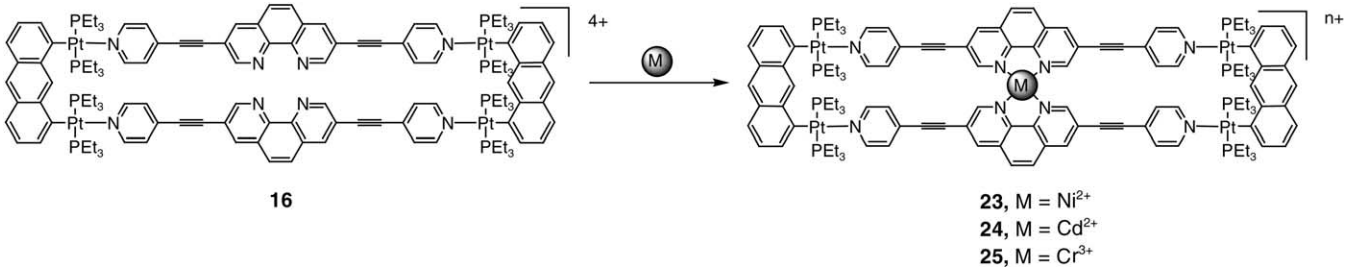

Scheme 10.

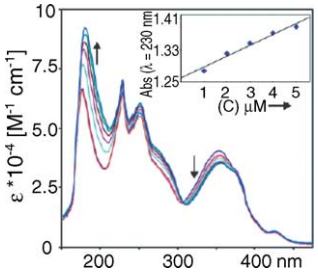

Fig. 2. Titration of **16** in MeOH with $Ni(NO_3)_2{\cdot}6H_2O$. Reprinted with permission from ref. [35]. © 2004 American Chemical Society.

Table 5
Binding constants[a] for **16** with Ni^{2+}, Cd^{2+}, and Cr^{3+}

	K
Ni^{2+}	$2.01 \pm 0.05 \times 10^7$
Cd^{2+}	$3.39 \pm 0.5 \times 10^4$
Cr^{3+}	$7.53 \pm 0.4 \times 10^3$

Data collected from ref. [35].

[a] Binding constants are obtained at 25 °C and 0.2 mM ionic strength in methanol. For free 1,10-phenanthroline, the binding constants are: Ni^{2+} (*K*, 8×10^7); Cd^{2+} (*K*, 5×10^5); Cr^{3+}, NA.

spectrum (Fig. 2). The results from Job's method and an ESI/MS study support a 1:1 complexation of **16** with Ni^{2+}, Cd^{2+} and Cr^{3+} ions to generate **23**, **24** and **25**, respectively (Scheme 10).

Further, the generation of an isosbestic point at 300 nm indicates that complexation occurs without perturbing the structure of **16**. The binding constants for **16** with metal ions are listed in Table 5. The observed equilibrium constants for complex formation with Ni^{2+}, Cd^{2+} and Cr^{3+} ions with **16** follow the same trend for affinity as those observed for free 1,10-phenanthroline with the same ions. However, complex **16** provides a supramolecular structure that endows the phenanthroline moiety with a preorganized architecture for metal binding as well as new optical properties.

Preliminary studies of complex **19** by means of ^1H NMR titration experiments [37] suggest that the oxalate guest molecule interacts with the NH_2 group of the $MeNH_2$ ligands in **19** in a concentration-dependent manner.

2.3. Synthesis of Ag- and Cu-based molecular rectangles

Similar to complex **20**, a ferrocene-based Ag-containing rectangle **26** was prepared by Lindner et al. [39] from the reaction of a $(\eta^5\text{-}C_5H_4C_2\text{-py})_2Fe$ moiety with $AgClO_4$ (Scheme 11). The intramolecular Ag–Ag distance in **26** is 3.50 Å. No long-range through-bond electronic communication between the ferrocene moiety is established in **26**, indicating that the Ag_2 cores fail to transmit the Cp–C≡C–py conjugation.

The ligand 4(2-pyridyl)-pyrimidine could be used as a versatile motif in the design and assembly of metallocyclic compounds, since its coordination sites are oriented ∼90° with respect to each other. In a study conducted by Beauchamp and Loeb [41], the Ag-based rectangle **27** was assembled by the reaction of 4(2-pyridyl)-pyrimidine with $AgCF_3SO_3$ in $MeNO_2$. The head-to-head plus tail-to-tail aggregation requires that the Ag(I) ions adopt different coordination geometries, i.e., distorted square planar and linear modes. The rectangular tetrameric cations form alternating layers with the $CF_3SO_3^-$ anions in the solid state.

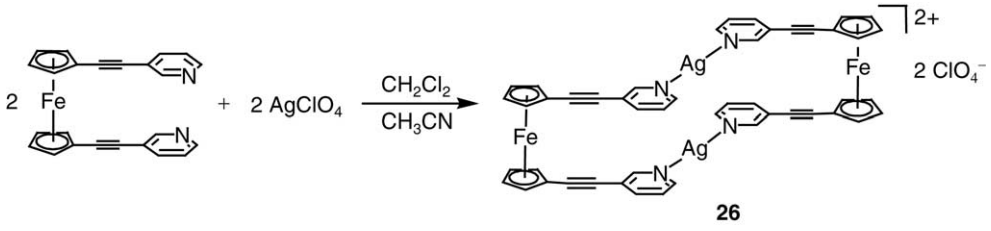

Scheme 11.

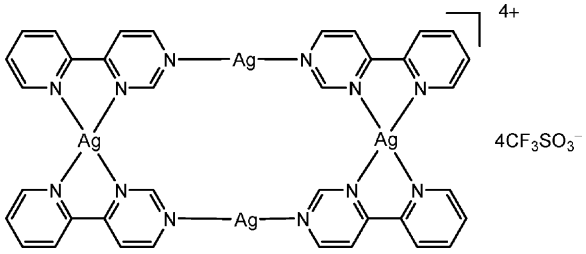

27

By taking advantage of the flexible conformation around the N–Si–Si–N skeleton in siloxane-containing pyridine, Jung et al. [42] were able to synthesize the molecular rectangles **28**–**31** by the slow diffusion of AgX ($X^- = NO_3^-$, ClO_4^-, PF_6^-, and $CF_3SO_3^-$) with this ligand (Scheme 12).

In **28**–**31**, the ligand connects two Ag(I) ions to form a 24-membered cyclic dimer that may be stabilized via intraligand face-to-face (π–π) interactions. The argentophilic interactions in **29**–**31** along with their related N–Ag–N angles are very sensitive to the bite size of each of the anions compared to **28**. Thus, the Ag–Ag distance (3.20 Å) is the shortest in **28** and the longest (3.81 Å) in **31**. In particular, **31** is transformed into a parallelogram to sustain the π–π interactions. Thus, a keen competition exists among the Ag–Ag, π–π and electrostatic interactions in **28**–**31**.

Hanton and co-workers [43] employed an interesting ligand based on a dibenzofuran spacer with exodentate thiopyridine arms, 4,6-bis(4′-pyridylsulfide)dibenzofuran in the formation of concave Ag_2L_2 rectangle **32**.

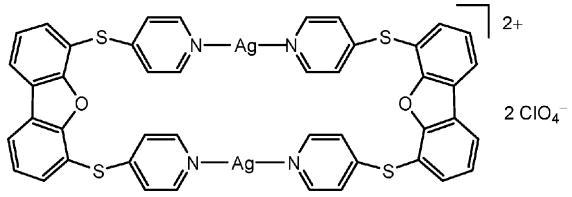

32

The pyridine arms of each ligand adopt a *syn* conformation and are bent with respect to the dibenzofuran spacer. Consideration was also given to the role of the ClO_4^- counter ions in **32**. Two opposite ClO_4^- anions weakly bridge the two Ag(I) ions in a bidentate manner possibly acting as clamps that serve to squeeze the Ag(I) ions together with Ag–Ag distance of 3.17 Å.

Su et al. [44] reported on the use of shape-specific designed ligands (1,3-bis(benzimidazol-1-ylmethyl)-4,6-dimethylbenzene $\mathbf{L}^1$, 1,3-bis(benzimidazol-1-ylmethyl)-2,4,6-trimethylbenzene $\mathbf{L}^2$, and 1,4-bis(benzimidazol-1-ylmethyl)-2,3,5,6-tetramethylbenzene $\mathbf{L}^3$) with different metal salts to produce a series of discrete molecular architectures of the Ag_2L_2 type: $[Ag_2\mathbf{L}_2^1](BF_4)_2$ (**33**) $[Ag_2\mathbf{L}_2^2](CF_3SO_3)_2$ (**34**) and $[CF_3SO_3^- – Ag_2\mathbf{L}_2^3]CF_3SO_3$ (**35**). The rectangle **33** possesses a two-fold rotational symmetry in which two *syn*-conformational $\mathbf{L}^1$ ligands are connected by two linearly coordinated Ag^+ ions.

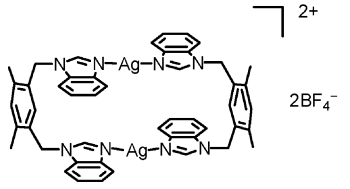

33

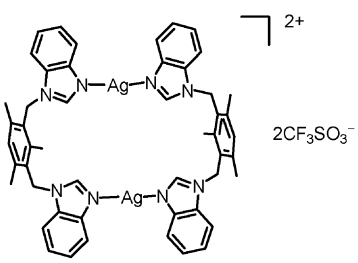

34

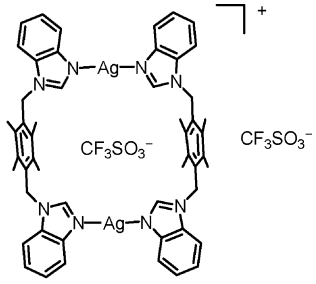

35

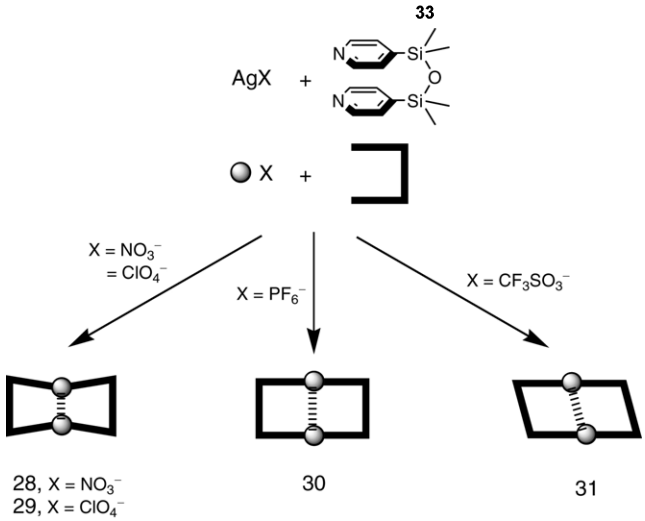

Scheme 12.

Lippert and co-workers [45] prepared the artificial nucleobases rectangle *trans*-[{$(NH_3)_2$Pt(9-MeA)(9-MeHx)Ag$(NO_3)(H_2O)$}$_2$Ag]$(NO_3)_3\cdot 6H_2O$ (**36**) by the reaction of *trans*-[$(NH_3)_2$Pt(9-MeA)(9-MeHxH)]$(NO_3)_2\cdot H_2O$ (9-MeA = 9-methyladenine, and 9-MeHx = 9-methylhypoxanthinate) in D_2O with three equivalents of $AgNO_3$. After the addition of a silver salt, the p*D* dropped to 2.6 and colorless crystals precipitated from the solution in 20% yield.

An example of the use of benzofuran ligands in the preparation of Cu-based rectangles **37** and **38** was provided by Hanton and co-workers [43]. From the reaction of 4,6-bis(4′-pyridylsulfide)dibenzofuran with $CuCl_2$, macrocycle **37**, bisected by a bridging chloride ion, is formed. Metallomacrocycle **38** is obtained by the reaction of 4,6-bis(methylsulfanylmethyl)dibenzofuran with CuI in a 1:2 ratio. In this case, the Cu_2I_2 moieties are incorporated into the

edge of the macrocycle **38**. The bridging Cu(II) ions in **37** adopted distorted square-pyramidal geometries and are coordinated in the basal plane. The molecular rectangle **38** possesses a center of symmetry comprised of two bichelating ligands, two Cu_2I_2 bridging moieties and a clearly defined cavity with two associated MeCN solvent molecules.

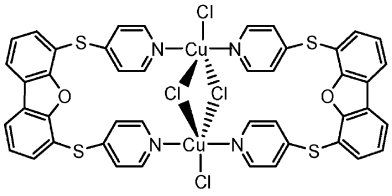

37

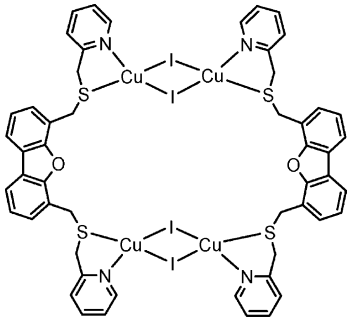

38

The assembly of metallo-cyclophane **39** was conducted by Martin and co-workers [46] by the addition of $[Cu(MeCN)_4]ClO_4$ to the Schiff-base ligand bis(pyridine-4,4′-diaminodiphenyl)methane and its derivatives. The molecular structure of **39** shows that the Schiff-base ligand adopts an unstrained conformation, reminiscent of that found in the uncoordinated "free" ligand. Compound **39** is arranged into a three-dimensional network in the solid-state by a combination of face-to-face π···π and edge-to-face C–H···π (3.5–3.9 Å) interactions.

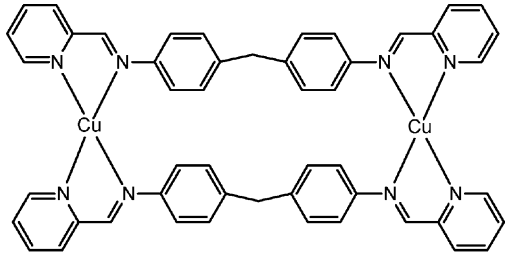

39

Enediyne compounds are known to possess attractive properties, such as DNA-damaging activity [47] or cycloaromatization [48]. Ueda and co-workers [49,50] demonstrated that the reaction of enediyne-type nitrogen ligands, 1,2-bis(2-pyridylethynyl)benzene, having bulky substituents with copper(I) ions leads to the self-organization of molecular rectangular boxes **40**–**42** in high yields (Scheme 13). X-ray analysis shows that each copper(I) ion in **40** (Fig. 3) has a distorted tetrahedral (N_2O_2) coordination, whereas the oxygen atoms are weakly coordinated to copper(I) ions. The two ligands of **40** and **41** are stacked above each other in a

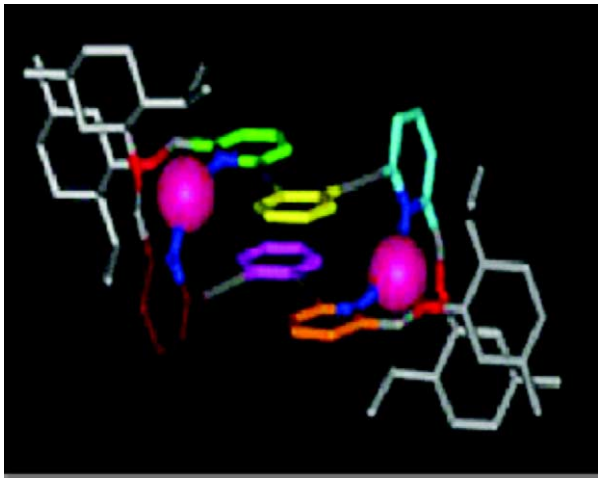

Fig. 3. Crystal structure of **40**. Reprinted with permission from ref. [49]. @ 2002 American Chemical Society.

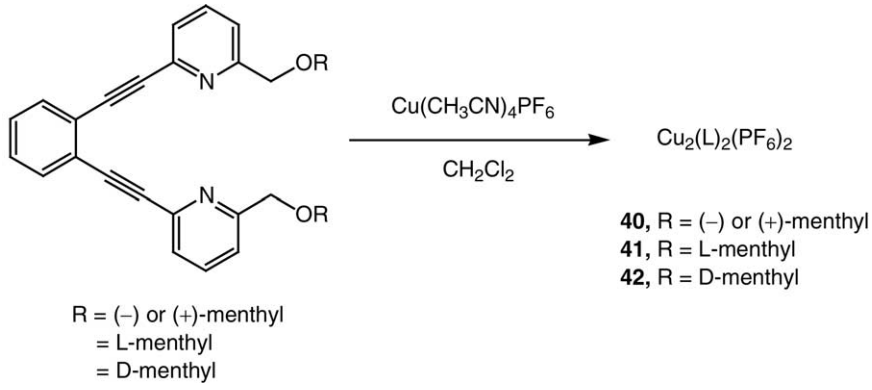

Scheme 13.

coplanar arrangement, with an interplane distance of about 3.5 Å consistent with π–π interactions.

2.3.1. Photophysics

The solid state UV–vis spectrum of **37** shows a broad asymmetric band at 693 nm [43] which was observed previously for five-coordinate $CuCl_2$ complexes of polypyridyl ligands [51].

The electronic absorption spectrum of **40** shows one absorption peak at 358 nm, which is assigned to an MLCT band [49]. The spectrophotometric titration of the optically active (menthyloxy)methyl substituted box with $Cu(CH_3CN)_4PF_6$ in dichloromethane shows clear isosbestic points, indicating the formation of a single species. The circular dichroism spectra were mirror images of each other. Additionally, a significant change in the optical rotations of the complexes in chloroform ((−)-menthyl substituted box $[\alpha]_D$ −446.9° (*c* 1.62); (+)-menthyl substituted box, $[\alpha]_D$ +418.4° (*c* 1.47)) implies that the reaction of the present ligands with the copper(I) ions proceed enantioselectively to afford enantiomerically pure complexes in solution.

2.3.2. Molecular recognition

In proceeding from **33** to **35**, the molecules exhibit an increasingly regular shape, especially with respect to the inner rectangular cavity [44]. This cavity, however, is arguably not a rectangular box because not all the sides are truly face-to-face parallel. The CH_3CN solvent molecules and BF_4^- anions are located around the metallacycle with almost negligible Ag···F (3.401 Å) and Ag···N (3.021 Å) interactions. In **34**, two $CF_3SO_3^-$ anions are attached to the macrocycle by weak Ag···O interactions and can be regarded as guest molecules. In **35**, on the other hand, one $CF_3SO_3^-$ anion is unambiguously located inside the rectangular metallacycle to give a $[CF_3SO_3^-–Ag_2L_2^3]^+$ cation, although it is crystallographically disordered (Fig. 4).

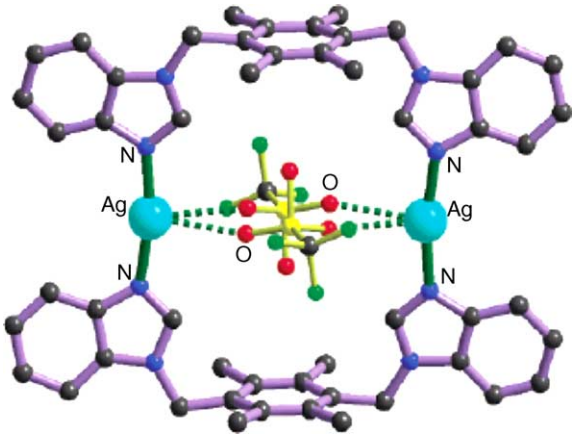

Fig. 4. Ball and stick representation of the $[CF_3SO_3^-–Ag_2\mathbf{L}_2^3]^+$ cation in **35** including the disordered $CF_3SO_3^-$ guest. Reprinted with permission from ref. [44]. © 2003 American Chemical Society.

2.4. Synthesis of Ni-, Zn- and Co-based molecular rectangles

Using the same strategy as shown in the preparation of ferrocene-based Pd- and Ag-rectangles (**20**, **26**), Lindner et al. [39] generated the Ni-based redox-active rectangle $[(\eta^5\text{-}C_5H_4C_2\text{-}4\text{-}py)_2Fe]_2Ni_2(NO_3)_4$ (**43**) by the reaction of $(\eta^5\text{-}C_5H_4C_2\text{-}py)_2Fe$ moiety with $[Ni(H_2O)_6](NO_3)_2$ (Scheme 14). The nickel complex **43** represents an unsymmetric paddlewheel in which the centres of the four Cp rings define a nearly ideal rectangle. A weak antiferromagnetic interaction between the nickel atoms in **43** was observed. Electrochemical studies reveal that an electron transfer from ferrocene to the nickel atoms occurs with no electronic communication between these ferrocene units.

In an attempt to design macropolycyclic molecules that function as receptors, Wozniak and co-workers [52] prepared a series of neutral bismacrocyclic Ni(II) compounds in which the macrocyclic units are linked by carbon bridges (Scheme 15). Large cavities are present in **44**, formed from macrocyclic fragments and two aliphatic chains. In particular, **44a** and **44b** form a unique 3D solid-state packing containing parallel channels thereby resembling the structure of an "organic zeolite".

Hunter et al. [53] combined a rigid bifunctional ligand of an appropriate size and zinc porphyrin "dimers" to synthesize complexes **45** and **46**, based on porphyrin coordination chemistry. The complexes **45** and **46** remain fully assembled down

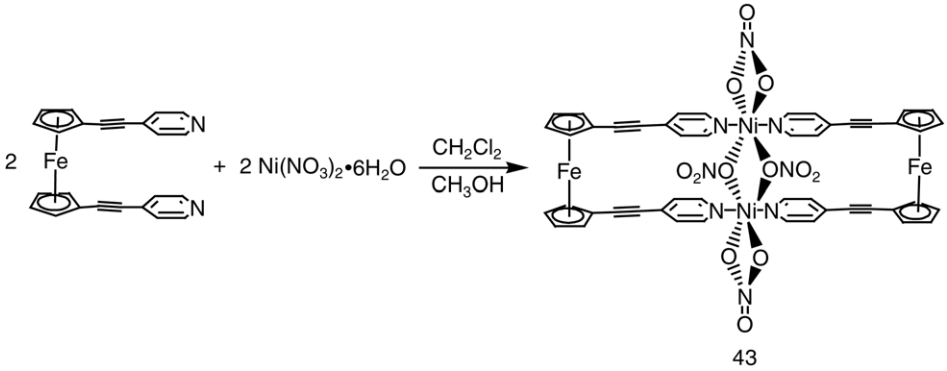

Scheme 14.

to concentrations below 10^{-7} M. These complexes are stable compared to a simple zinc porphyrin showing that cooperative self-assembly is occurring. Spectroscopic results indicate that the structures of these complexes are also closed; all of the coordination sites are occupied and there are no free end groups.

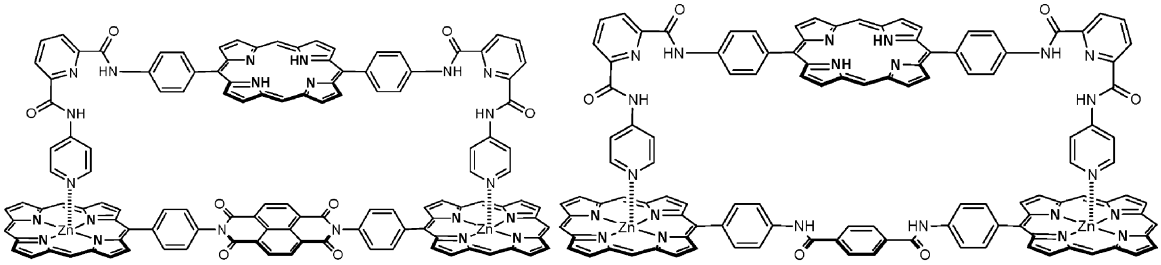

45 **46**

Dreos et al. [54] reported that boronic acids containing pyridinyl substituents such as 3-PyB$(OH)_2$ and 4-PyB$(OH)_2$ act as templates in the assembly of metallacycles [MeCo(DH)(DB(OMe)(3-Py))]$_2$ (**47**) and [MeCo(DH)(DB(OMe)(4-Py))]$_2$ (**48**), respectively. The macrocycles **47** and **48** are obtained by the reaction of an acidic residue with the O···H···O bridges of the methylaquacobaloxime units [$CH_3Co(DH)_2H_2O$] [55] and coordination of the pyridinyl group to the metal. The X-ray structure of **47** shows that two methylcobaloxime units are assembled by two B(OCH_3)(3-Py) residuals and can be considered to be a distorted "molecular rectangle". Complex **48** can be considered to be a rectangular box since the pyridinyl groups are also approximately perpendicular to the equatorial moiety. In fact, in **48**, the pyridinyl ligand is in an axial position, whereas in **47** it is in an equatorial position. The NMR spectrum shows no evidence of dissociation or the formation of polymeric species.

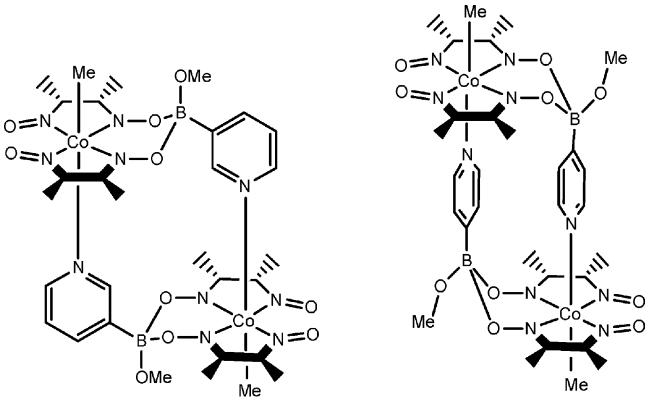

47 **48**

2.4.1. Photophysics

The UV–vis spectrum of **47** at pH 7 shows that pyridine is coordinated to the metal, Co [54]. This suggests that the complex obtained at pH 7 is a dimer but with the pyridine rings facing each other, not coplanar. The spectrophotometric titration of zwitterionic 4-pyridinyl boronic acid shows two acid–base processes, with isosbestic points at 210 and 260 nm, in the pH range 11.0–6.0, and at 256 nm, in the pH range 5.0–2.0, respectively. The relative pK_a values are 3.83 and 8.2. The lower value corresponds to ionization of the B$(OH)_2$ group, whereas the higher pK_a value is assigned to deprotonation of the pyridinyl group. UV–vis spectral studies confirm the ligation of pyridine at this pH value; the stepwise addition of 4-pyridinyl boronic acid to an aqueous solution of $CH_3Co(DH)_2H_2O$ at pH 10 causes spectral variations very similar to those observed for the coordination of pyridine to $CH_3Co(DH)_2H_2O$ (Fig. 5).

2.4.2. Molecular recognition

The binding properties of **44a** and **44b** toward selected electron acceptors such as quinone and TCNQ in solution have been studied by voltammetric techniques [52]. Upon mixing, the anodic peak corresponding to oxidation of the Ni(II) centers in **44a** and **44b** is shifted toward positive potentials. Simultaneously, the potential for the quinone reduction is significantly less negative. This indicates that the interactions between **44a** and **44b** and electron acceptors facilitate electron transfer with the electrode in solution. Based

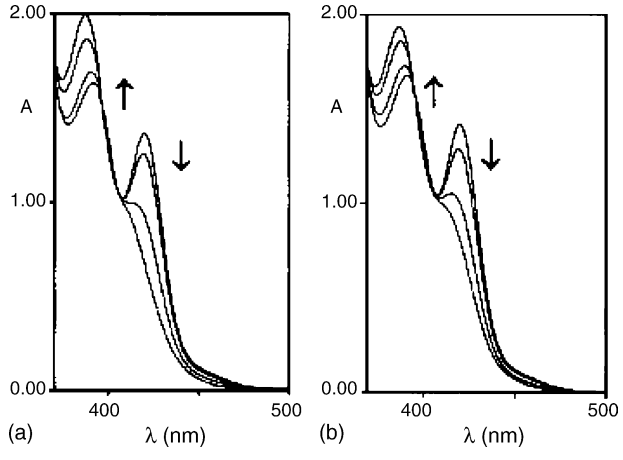

Fig. 5. Comparison of $CH_3Co(DH)_2H_2O$ spectral variation induced by coordination of 4-PyB$(OH)_2$ (a) and Py (b) at pH 10. Reprinted with permission from ref. [54]. © 2001 American Chemical Society.

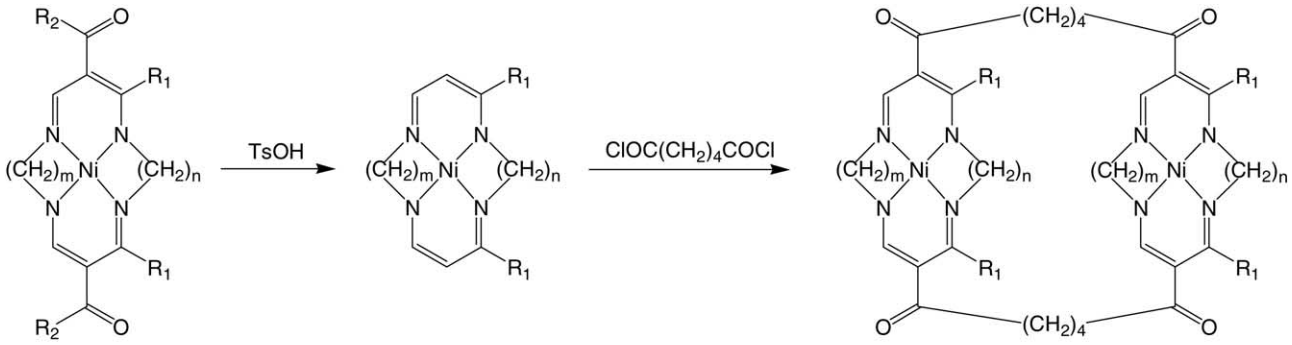

Scheme 15.

on available electrochemical data, the binding enhancement factor was found to be 6.0×10^{-3} and 6.5×10^{-2} for **44a** and **44b**, respectively. This indicates that upon reduction of the quinone, its binding strength to **44a** is increased by ca. 164 times. Only a 15-fold increase was noted for macrocycle **44b**, with a smaller cavity. In the case of a different electron acceptor, TCNQ, this increase was negligible, 1.8 and 1.5 times for **44a** and **44b**, respectively. In addition, the C–H···π or non-polar character of the inside of the cavity influences the affinity of the macrocycle toward the guest in solution.

3. Molecular rectangles containing sulphur-, oxygen- and other atoms-bridged ligands

3.1. Synthesis of Re-based molecular rectangles

Hupp and co-workers [56] described the synthesis of sulphur-bridged rectangles **49**–**52** by the reaction of $Re(CO)_5OTf$ (OTf = trifluoromethane sulphonate) with various alkyl and aromatic thiols at room temperature followed by refluxing with pyrazine or 4,4′-bpy. The synthesis of **49**–**52** is detailed in Scheme 16.

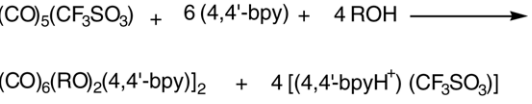

Scheme 17.

Sullivan and co-workers [57] reported on a class of molecular rectangles $[Re_2(CO)_6(RO)_2(4,4'\text{-bpy})]_2$ (**53**, R = OH, OCH_3, OCH_2CH_3, OCH_2CH_2OH) based on *fac*-$Re(CO)_3$ corners containing 4,4′-bipyridine bridges as one side and two alkoxy or hydroxy bridges as the other. These compounds were prepared by the reaction of the precursor $Re(CO)_5(CF_3SO_3)$ with 4,4′-bpy in presence of alcohols or water to afford quantitative yields of yellow microcrystals (Scheme 17).

The self-assembly of rectangles **54**–**57** from $Re_2(CO)_{10}$ as the starting material was carried out in high-yield using a solvothermal method [58,59]. When $Re_2(CO)_{10}$ was treated with the bipyridyl ligands (pyrazine (pz), *trans*-1,2-bis(4-pyridyl)ethylene (bpe), 1,4-bis-[2-(4-pyridyl)ethenyl]benzene (bpeb) and 4,4′-bipyridine (bpy)) in the presence of higher aliphatic alcohols, alkoxy bridged molecular rectangles $[\{(CO)_3Re(\mu\text{-}OR)_2Re(CO)_3\}_2(\mu\text{-}L)_2]$

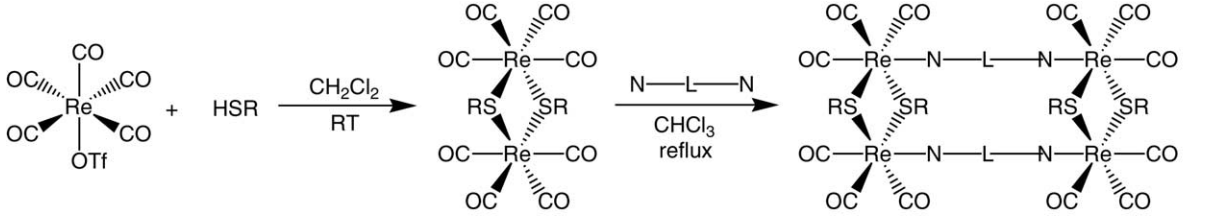

Scheme 16.

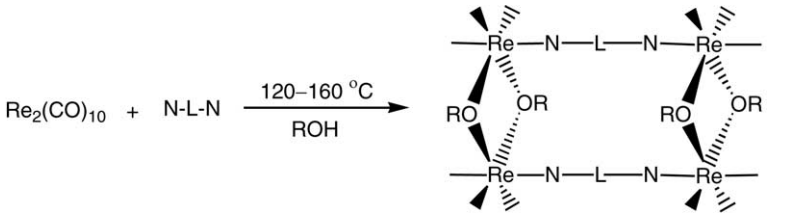

54, N-L-N = pz, R = -C_4H_9, -C_8H_{17}
55, N-L-N = bpe, R = -C_4H_9, -C_8H_{17}
56, N-L-N = bpeb, R = -C_4H_9, -C_8H_{17}
57, N-L-N = bpy, R = -C_4H_9, -C_8H_{17}, -$C_{12}H_{25}$

Scheme 18.

(**54**–**57**) are obtained (Scheme 18). The more hydrophobic nature of the rectangles containing an octyl group compared to those carrying a butyl group enhances their solubility in less polar solvents.

3.1.1. Photophysics

The UV–vis spectra of **49**–**52** [56] show a ligand centred transition in the regions 328–386 nm. For **49**, **51** and **52**, the MLCT transition is observed in the low energy region at 400 nm as a shoulder and for **50** it appeared at 482 nm. The rectangles **49**–**52** display a reversible wave at 0.48 V and an irreversible redox wave at 0.80 V, which are assigned to metal or metal/sulphur oxidation and $Re^{I/II}$ oxidation, respectively. These complexes also exhibit reversible reduction at −1.23 and −1.64 V versus ferrocene for pyrazine and −1.60 and −1.81 V for bipyridine ligands.

The UV–vis spectra of oxo-bridged rhenium rectangles $[Re_2(CO)_6(RO)_2(4,4'\text{-bpy})]_2$ (**53**) (R = OH, OCH_3, OCH_2CH_3, OCH_2CH_2OH) [57] are characterized by a sharp, intense π–π^* transition at ca. 240 nm and a broad band around 380 nm, assigned to the $d\pi(Re)$–π^*(bpy) MLCT transition. The ligand π–π^* transition is insensitive to structural changes, whereas the MLCT band is red-shifted for the rectangles. In **53**, luminescence is observed only in the solid state and not in solution. The non-emissive characteristics in solution can be attributed to an enhanced nonradiative decay via the torsional motion of 4,4′-bpy and/or its origin in a LLCT excited-state of the alkoxide donor and bpy acceptor orbitals. A cyclic voltammetry study of $[Re_2(CO)_6(OCH_3)_2(4,4'\text{-bpy})]_2$ showed two irreversible one-electron 4,4′-bpy reductions at −1.09 and −1.28 V versus SCE and one irreversible Re-based oxidation at +1.34 V.

Spectral absorption studies of **54**–**56** [58] reveal the existence of π–π^* and MLCT transitions in the higher and lower energy regions, respectively. A red shift of 61 nm (from 398 to 459 nm) was observed in the MLCT transition of **54**–**56** on changing the ligand from bpe to pz. Excitation of **54**–**56** at their MLCT results in emission at 440–490 nm in CH_3CN and CH_2Cl_2. However, both the free ligands and the rectangles **54**–**56** exhibit an emission around the same region, the observed emission for **54**–**56** may originate from the MLCT band, primarily involving bridging ligands. Thus, the excited state lifetimes of **54**–**56** are in the range of 10–15 ns at room temperature. Cyclic voltammetric data for **54**–**56** show that two reductions appear at −0.73 to −1.28 V, corresponding to the successive reduction of the bridging ligands and one reduction at −1.35 to −1.50 V versus SCE to the Re metal. The oxidation peaks observed at 1.00–1.65 V may be attributed to the oxidation of the Re metal center. Since the alkoxy bridge remains a good electron donor in **54**–**56** no redox potential is detected in the range −2.00 to 2.00 V.

The absorption spectrum of $[\{(CO)_3Re(\mu\text{-}O(CH_2)_{11}CH_3)_2Re(CO)_3\}_2(\mu\text{-bpy})_2]$ (**57c**) in CH_3CN [59] shows an intense band at 241 nm with a shoulder at 266 nm and a broad band at 385 nm. The bands at 291 and 266 nm are assigned to the ligand-centred (LC) and that at 385 nm to the MLCT transition, respectively. In 10% H_2O–90% CH_3CN, the LC transition at 241 nm has a reduced intensity, while the shoulder at 266 nm becomes more pronounced. When the water content is increased from 20 to 90%, the bands at 241 and 266 nm are shifted to 248 and 272 nm, respectively, with a concomitant increase in intensity, whereas the MLCT band at 385 nm is red-shifted by 5 nm on the addition of water. The absorption spectra hints at a scattered light pattern as a function to the fourth of the frequency that tails down to 600 nm, and these results strongly suggest nanoparticle suspensions [60].

The Re(I) complexes **57** are faintly emissive. The addition of water leads to an enormous enhancement in emission intensity (Fig. 6) for **57c**, while the effect is moderate with $[\{(CO)_3Re(\mu\text{-}O(CH_2)_3CH_3)_2Re(CO)_3\}_2(\mu\text{-bpy})_2]$ (**57a**) and $[\{(CO)_3Re(\mu\text{-}O(CH_2)_7CH_3)_2Re(CO)_3\}_2(\mu\text{-bpy})_2]$ (**57b**). Although, the shift in MLCT absorption band is small, the corresponding emission maximum is substantially blue-shifted with a higher quantum yield (Table 6). These results indicate the presence of alkyl chain aggregates which expel solvent molecules, and the aggregation leads to less vibrational motion. Tang and co-workers [61] also observed similar spectral changes in the aggregation of siloles.

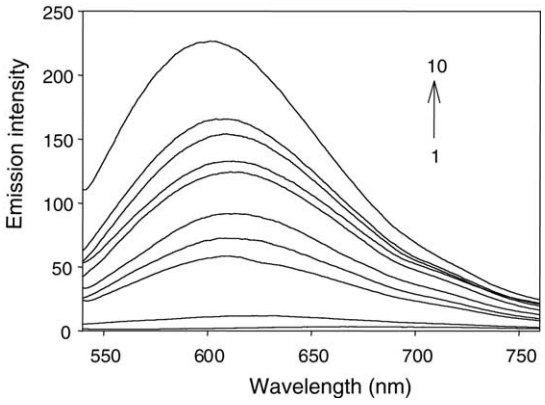

Fig. 6. Emission enhancement of **57c** in CH_3CN upon increasing water content: (1) 0%, (2) 10%, (3) 20%, (4) 30%, (5) 40%, (6) 50%, (7) 60%, (8) 70%, (9) 80%, and (10) 90% (λ_{ex} = 390 nm). Reprinted with permission from ref. [59]. @ 2002 American Chemical Society.

A light scattering study of **57c** indicated an average aggregate mass of the Re(I) rectangle **57c** in 50% aqueous CH_3CN (v/v) of 1.43×10^6 with an average diameter of 262 nm. The addition of water favours the aggregation of **57c**, resulting in an enormous enhancement in luminescence. Thus amphiphilic molecules carrying long alkyl chains can undergo aggregation and this affects the luminescence of the molecule, thus extending the scope of its applications [61,62].

3.1.2. Molecular recognition

Considering the van der Waals radii of sulphur- or oxygen-bridged rectangles **49**–**57** [56–59], the interplanar spacing is too small to allow the resulting cavity to function as a receptor site, even for planar molecules.

To achieve molecular recognition of the luminescent rectangle **57**, the reaction of **57c** with various quinones was studied by the luminescence quenching technique [59]. The quenching reaction is efficient and the rate constant for quenching, k_q, values are in the range 2.0×10^8 to $3.8 \times 10^{11}\ M^{-1}\ s^{-1}$. The deviation from linearity in the Stern-Volmer plot implies that quenching occurs via a static process. The binding constants of quinones with **57c** can be evaluated using the Benesi–Hildebrand equation for 1:1 host–guest interactions. Analysis of the data for **57c**, for an interaction with methyl-*p*-benzoquinone, gives a binding constant of $4.1 \times 10^2\ M^{-1}$. ^1H NMR studies of **57c** with increasing concentrations of methyl-*p*-benzoquinone in a 50% (v/v) THF-d_8/D_2O mixture lead to downfield shifts of the H^3 and H^2 protons of the pyridyl group of **57c** when a 0.075 M concentration of methyl-*p*-benzoquinone was used. The chemical shifts of the alkoxy protons remain largely unchanged upon the addition of quinone. This study further supports the conclusion that quinone interacts closely with the pyridyl group of **57c**.

Table 6
Wavelength of emission maximum (λ^{em}_{max}), emission quantum yield (Φ), and lifetime (τ) of **57c** in various CH_3CN–H_2O (v/v) mixtures

Serial number	Solvent, CH_3CN (%)	Composition, H_2O (%)	λ^{em}_{max} (nm)	Φ ($\times 10^{-3}$)[a]	τ (ns)
1	100	–	666	0.39	11
2	90	10	634	0.46	13
3	80	20	612	1.64	120
4	70	30	611	1.73	124
5	60	40	613	2.06	135
6	50	50	613	2.37	137
7	40	60	612	2.58	140
8	30	70	611	3.10	167
9	20	80	604	4.74	176
10	10	90	602	6.54	212

Data collected from ref. [59].
[a] Emission quantum yield measured at 298 K with reference to $Ru(bpy)_3^{2+}$: Φ_{em}, 0.042; λ_{ex}, 409 nm.

3.2. Synthesis of other metal-based molecular rectangles

Mirkin and co-workers [63] demonstrated that the "weak-link" approach to macrocycle synthesis is broadly applicable to the preparation of structures with tailorable properties. They reported a one-pot and high-yield approach to the synthesis of the binuclear macrocycle **58** from structurally flexible hemilabile phosphino aryl-ether ligands as shown in Scheme 19. Derivatives of these macrocycles were also assembled.

The "weak-link" synthetic strategy was utilized in the construction of metallomacrocycles using several Pd(II) and Rh(I) complexes with a variety of hemilabile ligands [63,64]. Some of the macrocycles **59a–c** are shown in Scheme 20. However, Rh(I) exhibits some notably different characteristics, in that it can accommodate η^6-arene interactions which leads to intermediates that are observed in the case of Pd(II).

Another example of the preparation of the condensed macrocycle **60** containing phosphinothioether ligands via the "weak-link" approach has also been reported [65]. The thioether-based macrocycle can open via a halide-induced ring opening reaction whereby a halide source is used to break the Rh^I–S bonds (Scheme 21). In **60,** each Rh^I metal centre is in a square-planar *cis*-phosphine, *cis*-thioether geometry, and the parallel–planar arene rings are 3.51 Å apart.

Yamamoto and co-workers [66] were able to synthesize supramolecular complexes bearing arene and cyclopentadienyl groups and derivatives thereof. The reactions of $[CpMCl_2]_2$ (M = Rh, Ir) with a bidentate ligand (L = pyrazine; L′ = diisocyanide) give $[CpMCl_2L]_2$ and $[CpMCl_2L']_2$, which can be converted into tetranuclear complexes $[Cp_2M_2Cl_2(L)(L')]_2(OTf)_4$ (**61**, M = Ir; **62**, M = Rh,) containing different ligands on treatment with Ag(OTf) (Scheme 22).

The self-assembly of platinum-containing rectangles **63**–**67** has been reported from the laboratory of Stang and co-workers [67]. The authors employed a rigid, dicarboxylate-based oxygen donor with 1,8-bis(*trans*-$Pt(PEt_3)_2(NO_3)$)anthracene to form molecular rectangles **63**–**67** as shown in Scheme 23.

^1H NMR analyses of **63**–**67** revealed, the dicarboxylates are incorporated into the product. Further, X-ray structure

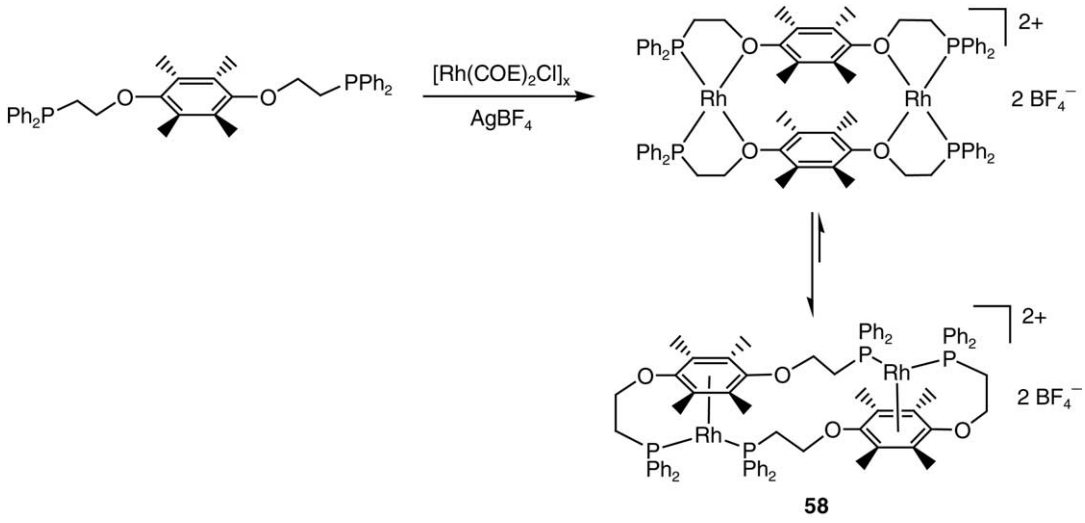

58

Scheme 19.

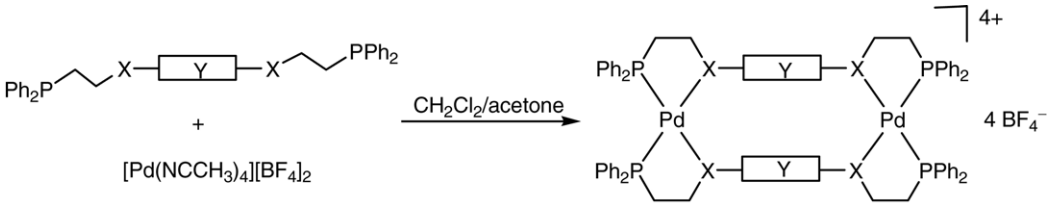

59a, X = O, Y = 1,4-$C_6(CH_3)_4$
59b, X = O, Y = 1,4-C_6H_4
59c, X = S, Y = 1,4-C_6H_4

Scheme 20.

analyses of **63** and **64** inferred the existence of disordered solvent molecules in each case. The structures of **63**, **65**–**67** are slightly bowed in the middle, due to the steric repulsion of the triethylphosphines. No channels are observed in **66** due to offset packing. These neutral self-assemblies **63**–**67** are smaller in length in comparison to the other ionic Pt-based rectangles synthesized with larger N-donor linkers.

Andruh and co-workers [68] were able to synthesize Cu-based rectangles, **68**–**71** by employing bis(4-pyridyl) exo-bidentate ligands such as 4,4′-bipyridine, 1,2-bis(4-

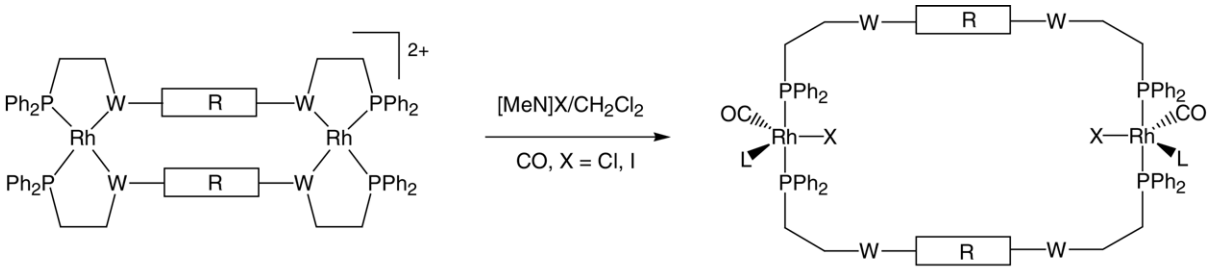

W = S, R = *p*-C_6H_4
W = O, R = *p*-$C_6(CH_3)_4$

60a, W = S, X = Cl, L = none, R = *p*-C_6H_4
60b W = S, X = I, L = CO, R = *p*-C_6H_4
60c, W = O, X = Cl, L = none, R = *p*-$C_6(CH_3)_4$
60d, W = O, X = Cl, L = none, R = *p*-C_6H_4

Scheme 21.

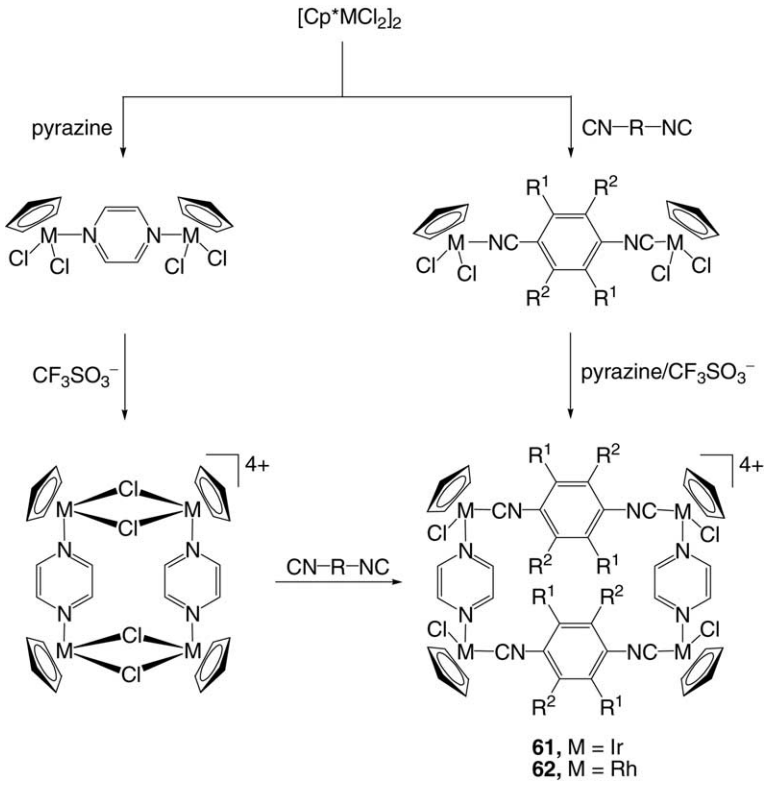

Scheme 22.

pyridyl)ethylene, and 1,2-bis(4-pyridyl)ethane (bpeta), and an unsymmetrical linker IN^- (IN^- = isonicotinato ion) with binuclear precursor $[L(\mu\text{-}OH)Cu_2](ClO_4)_2$ (L = 2,6-bis[*N*-2-pyridylethyl]formimidoyl)-phenolato) complex (Scheme 24). The X-ray structures of **68** and **69** showed close face-to-face π–π stacking of the 4-pyridyl rings. The distances associated with the π-interactions of the pyridyl moieties are in the range 3.51–3.78 Å for **68**, and 3.54–3.64 Å for **69**. The process appears to be favored by the preference of copper(II) in **70** for the square pyramidal stereochemistry, and not by π–π stacking interactions between the pyridyl rings. The copper(II) ions in **71** have a square pyramidal

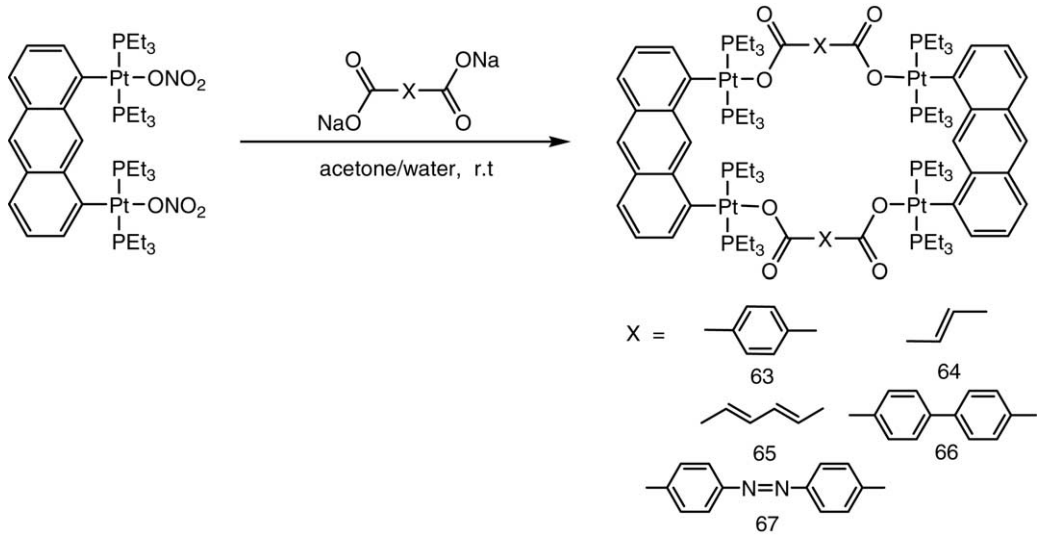

Scheme 23.

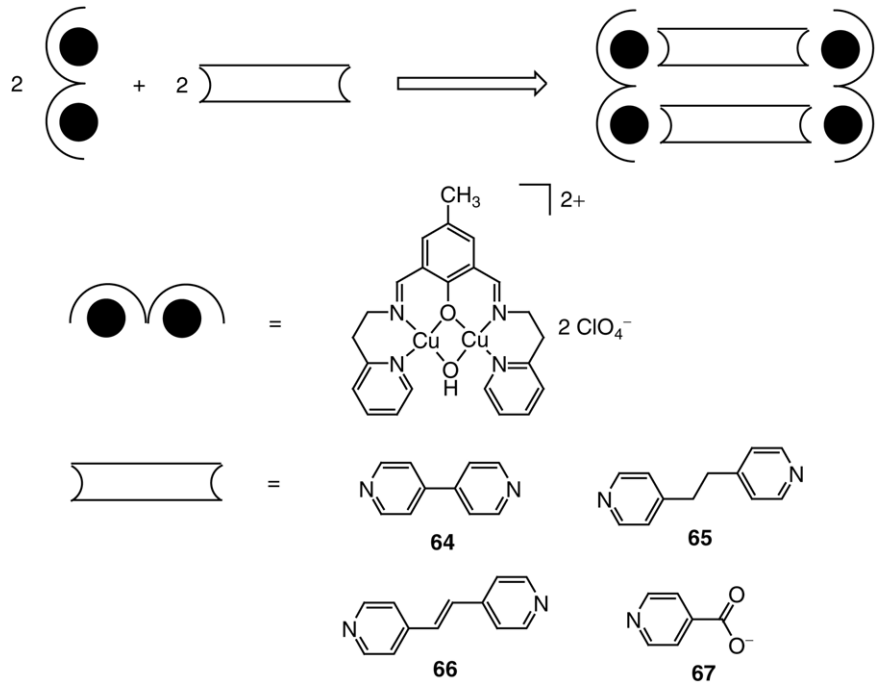

Scheme 24.

stereochemistry but different coordination environments. The basal plane is the same for both copper(II) ions in **71**: two nitrogen atoms from the Schiff-base, and the two oxygen atoms arising from the pre-existing bridges in the binuclear moieties.

A number of thiosemicarbazones, thiocarbazones and their metal complexes were reported to be active in cell destruction as well as the inhibition of DNA systems. Cheng et al. [69] reported the incorporation of such types of ligands for binding to an octahedrally coordinated transition metal via self-assembly. The interaction of $CuCl_2{\cdot}2H_2O$ with bis[phenyl(2-pyridyl)methanone]thiocarbazone in DMF affords a tetranuclear metal complex **72**. Magnetic susceptibility studies indicated a strong antiferromagnetic coupling among the Cu(II) ions. From the X-ray crystallographic studies, the complex **72** is described as a centric symmetric dimer of dicopper(III) moieties. The geometry of the Cu atom is square pyramidal with respect to the pyridine nitrogen atom, thiocarbazone nitrogen atom, the sulphur atom and the chlorine atom, comprising a basal plane.

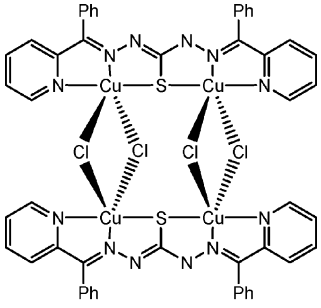

72

Maverick et al. [70] reported on some binuclear complexes derived from polydentate ligands. A dichloromethane solution of *m*-$XBAH_2$, and $NBAH_2$ ($XBAH_2$ = 3,3′-[1,3-phenylenebis(methylene)]bis(2,4-pentanedione); $NBAH_2$ = 3,3′-[2,7-naphthalenediylbis(methylene)]bis(2,4-pentanedione)) on treatment with an aqueous solution of $Cu(NH_3)_4^{2+}$ resulted in the growth of crystals of Cu_2(*m*-XBA)$_2$ (**73**) and $Cu_2(NBA)_2$ (**74**), respectively. The well-defined size and shape of the inner cavity in **73** and **74** is controlled by the side organic linkage to adapt various types of guest molecules.

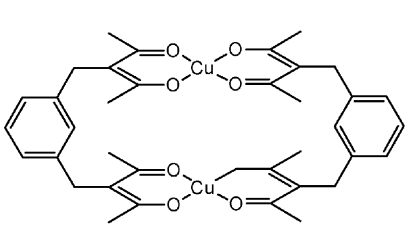

73

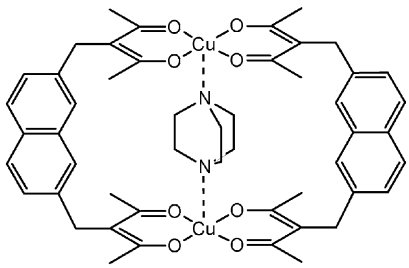

74

The synthesis of the bis(β-ketoenamine) ligand, or 5-*tert*-butyl-*m*-xylylenebis(acetylacetoneimine)(3,3′-[5 - (1, 1-dimethylethyl)-1,3 - phenylenebis - (methylene)]- bis(4-amino-3-penten-2-one)), and the properties of three of its cofacial binuclear metal complexes **75**–**77** (Cu, Ni and Pd) were reported by Maverick and co-workers [71]. Complexes **75**–**77** dissolve in halogenated solvents with solubilities in the order Cu > Pd > Ni. The possibility of isomerism in **75**–**77** was also described. The binuclear complexes **75**–**77** exhibit several improvements in redox behaviour compared with simple mononuclear β-ketoenamine complexes.

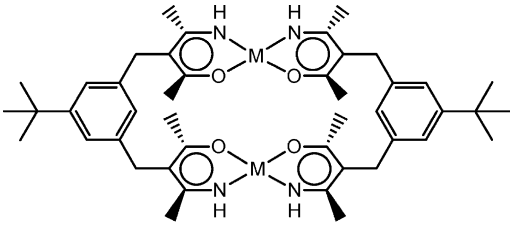

75, M = Cu
76, M = Ni
77, M = Pd

The incorporation of redox-active components, such as ferrocene, into a macrocyclic ligand framework introduces the possibility of the host being capable of electrochemically recognising species. Using the strategy of a metal-directed synthesis, Beer and co-workers [72] prepared the macrocycles **78**–**83** by the reaction of ferrocenyl secondary amines with carbon disulfide, potassium hydroxide and transition metal (Zn, Cu, Ni) acetates in high yields (Schemes 25 and 26). The electrochemical properties of **78**–**83** exhibit a single reversible oxidation wave at $E_{1/2} = 0.25$ V versus Ag/AgCl suggesting that all ferrocene moieties are oxidized in a single step and are electrochemically independent of one another. The bis-copper(II) analogue **79** displays a broad oxidation redox wave at $E_{1/2} = 0.26$ V versus Ag/AgCl resulting Cu(II)/Cu(III) dithiocarbamate redox couple which overlaps with the respective ferrocene oxidation couple. Two oxidation couples are observed for **80** in which a reversible wave at $E_{1/2} = 0.26$ V for the ferrocene redox couple and an irreversible oxidation at $E_{pa} = 0.31$ V versus Ag/AgCl for the Ni(II)/Ni(IV) dithiocarbamate oxidation process. The macrocycle **78** is reversibly oxidized in a single step at $E_{1/2} = 0.35$ V versus Ag/AgCl and **81** displays two oxidation waves but only one return reduction wave is observed.

A rare example of cyclic 2:2 coordination complexes of nitroxide radical with Cu(II), Mn(II), Ni(II) and Co(II) (**84**–**87**), as shown in Scheme 27, was reported by Field and Lahti [73]. These complexes are isostructural and crystallographically isomorphous. All these complexes show strong antiferromagnetic metal–ligand exchange properties.

Kahn and co-workers [74] prepared the Mn-based rectangle ((bis{[(*p*-nitronyl nitroxidephenyl)diphenylphosphine-oxide]bis(hexafluoroacetylacetonato)-manganese-(II)} (**88**) by the addition of the free radical phosphine oxide to

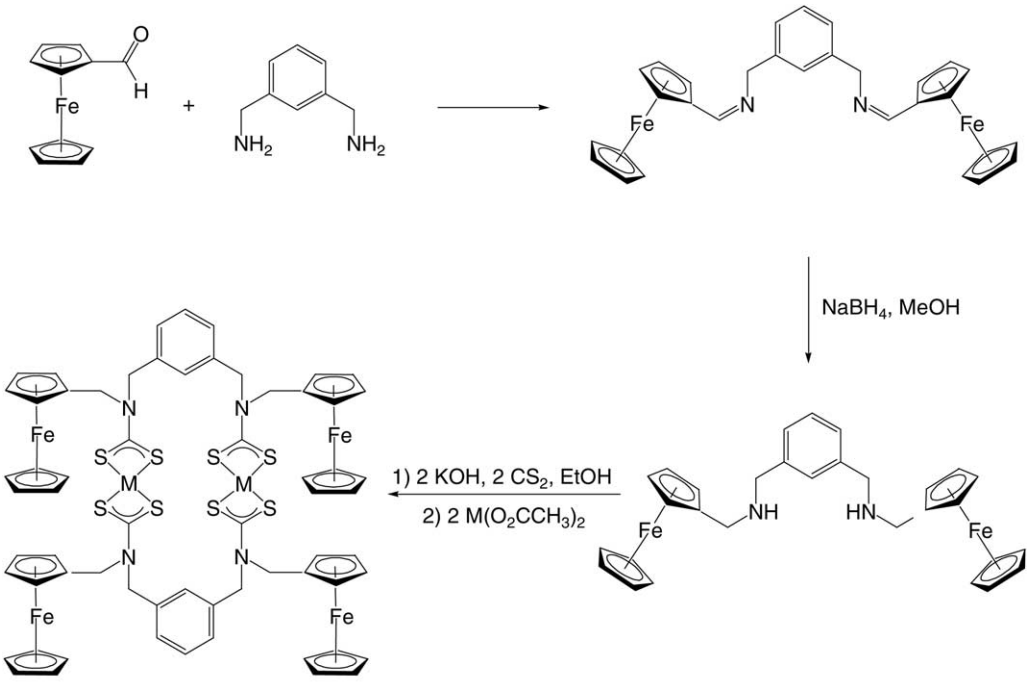

78, M = Zn
79, M = Cu
80, M = Ni

Scheme 25.

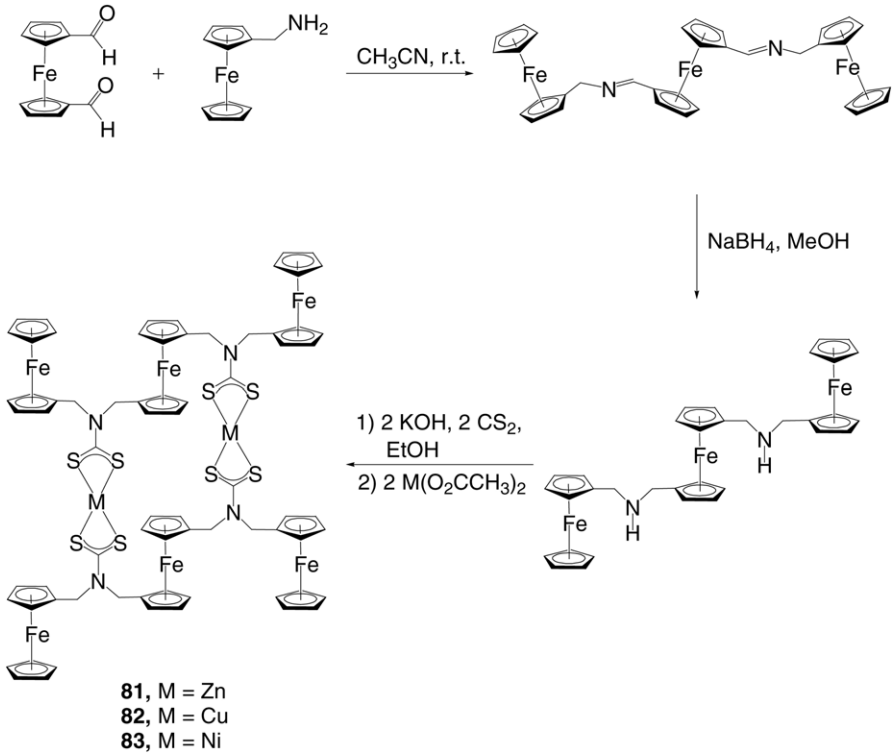

Scheme 26.

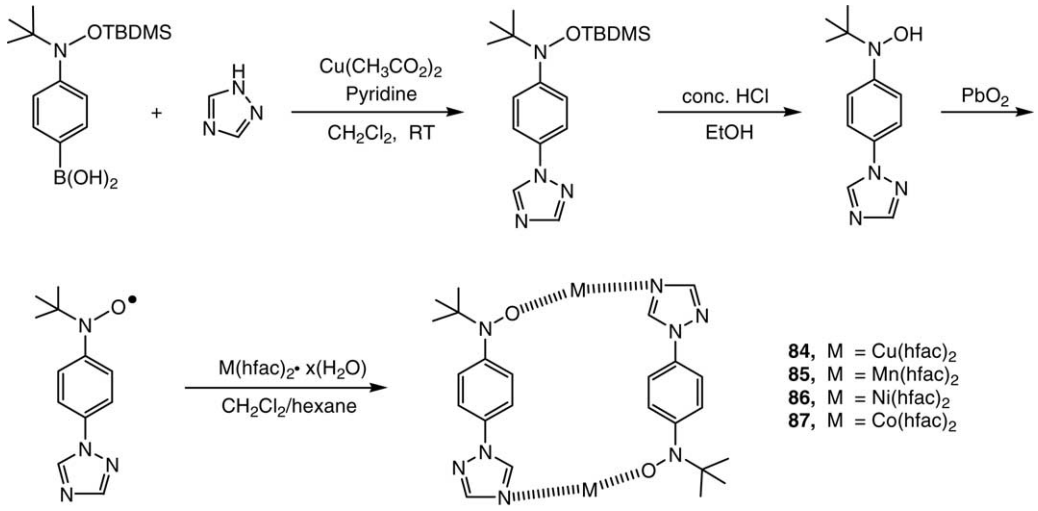

Scheme 27.

$Mn(hfac)_2$ (Scheme 28). The formation of **88** is facilitated by the topology of phosphine oxide. The magnetics of **88**, indicating little interaction between pairs, is also instructive as a model for extended systems or compounds with multiple paramagnetic ligands.

Metal alkoxides [M(OR)*x*] were found to have great utility as precursors in solution (i.e., sol–gel) or gaseous (i.e., metallo-organic vapor deposition) routes to thin films of ceramic materials. The generation of the metal alkoxide rectangle $\{[(OPr^i)_2(\mu\text{-}OPr^i)Ti]_2(\mu\text{-}DHP)\}_2$ (**89**) was examined by Boyle et al. [75] using 4,6-dihydroxypyrimidine ($DHPH_2$) as a selective bridging ligand with $Ti(OPr^i)_4$ in pyridine.

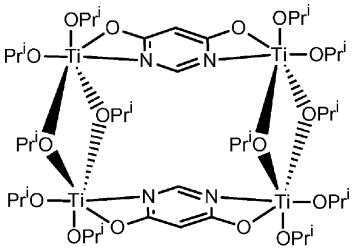

89

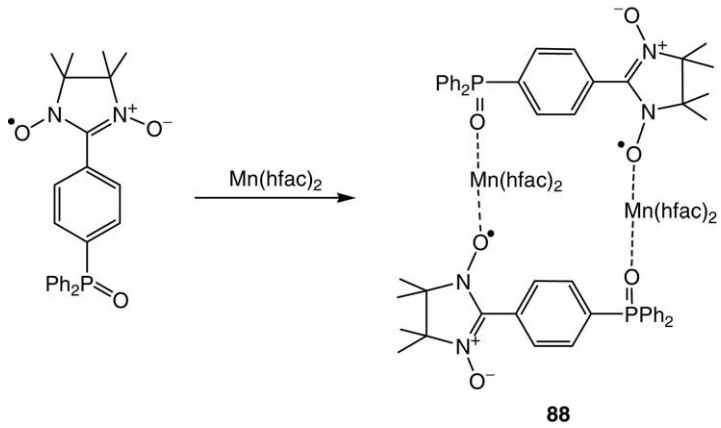

88

Scheme 28.

Duhme [76] prepared an interesting example of the Mo-based rectangle **90**. The reaction of dinucleating ligand *N*,*N*′-bis(2,3-dihydroxybenzoyl)-α,α-diaminopropane (H_4-1) with molybdate results in the formation of the rectangle Δ,Λ-$[\{MoO_2(H_4)\}_2]^{4-}$ as confirmed by NMR and X-ray analysis. From the following facts, this ligand can be summarized as follows: (i) the molybdenum building block requires a ligand with planar bidentate subunits. On reaction with molybdenum, two oxo ligands remain coordinate to the molybdenum atom with two adjacent coordination sites of the octahedral metal centre. The four vacant coordination sites allow the binding of two catecholamides, leading to the formation of molecular rectangle, (ii) the propyl spacer is sufficiently short to prevent monomer formation, and (iii) the spacer is still sufficiently flexible to allow bending of the ligand.

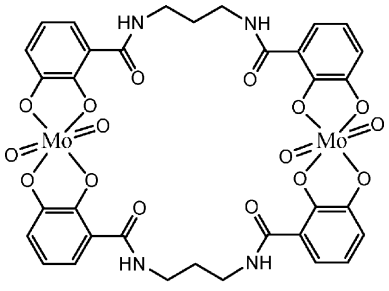

90

The organoruthenium complex **91**, containing bidentate oxygen ligands and 4,4′-bipyridine, was reported by Fink and co-workers [77]. The reaction of the precursor complex $[Ru_2(\mu\text{-}\eta^4\text{-}C_2O_4)(MeOH)_2(\eta^6\text{-}p\text{-}Pr^iC_6H_4Me)_2]^{2+}$ with 4,4′-bipyridine gives the macrocyclic cation $[Ru_4(\mu\text{-}\eta^4\text{-}C_2O_4)_2(\mu\text{-}\eta^1\text{:}\eta^1\text{–bipy})_2(\eta^6\text{-}p\text{-}Pr^iC_6H_4Me)_4]^{2+}$ (Scheme 29). A single-crystal X-ray analysis of **91** revealed a macrocycle with alternating oxalate and 4,4′-bpy bridges between the ruthenium atoms. As this complex possesses crystallographic C_2 symmetry, the two-oxalato planes are parallel to each other. The two pyridine rings of each 4,4′-bpy are inclined toward one another but are not coplanar. The quality of the crystal and the problems associated with disorder of the anion led to considerable errors in the bond lengths and angles.

3.2.1. Photophysics

The electronic spectrum of **67** exhibits a near-UV transition, which is red-shifted relative to NaOOC–C_6H_4N=NC_6H_4–COONa linker and very slightly blue-shifted relative to 1,8-bis(*trans*-$Pt(PEt)_3)_2(NO_3)$anthracene [67]. The absorbance per NaOOC–C_6H_4N=NC_6H_4–COONa linker unit increases significantly upon rectangle formation; likewise, the anthracene-based absorbance, centered around 280 nm, also increases significantly.

The electronic spectrum of **73** [70] shows two d–d transition bands at 518 and 646 nm. The copper atoms in this complex behave electronically much like an isolated $Cu(acac)_2$ unit.

3.2.2. Molecular recognition

The electronic reactivity of solutions of **73** in chloroform was studied with and without added pyridine [70]. Complex **73** exhibits two d–d transition bands that appear at 518 and 646 nm. The new d–d transition band at 635 nm is formed in **73** on the addition of pyridine with the colour changing from olive green to bright yellow-green. As the space between the copper atoms is too small to accommodate pyridine, the evidence is consistent with the formation of new species as **73** $(py)_2$. ^{1}H NMR spectroscopy studies revealed the association of H_2O molecules with **73** in $CHCl_3/CDCl_3$ mixtures showing significant broadening of the $CHCl_3$ resonance, consistent with specific outer-sphere interactions with $CHCl_3$. The electronic absorption spectrum of **74** shows a d–d transition in the 450–800 nm region. An olive green solution of **74** turns turquoise on the addition of nitrogen bases. The binding constants (Table 7) were calculated using the changes in absorbance at 500–600 nm.

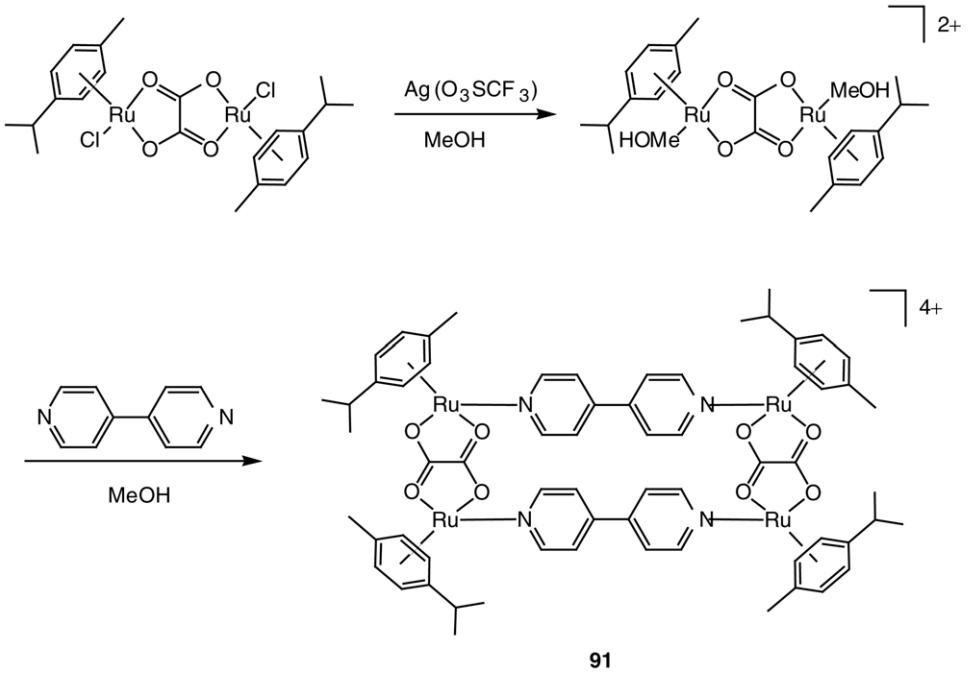

Scheme 29.

The X-ray analysis of **74**(μ-2,5-Me_2pyz)·4CH_2Cl_2 demonstrated that pyrazine coordinates intramolecularly to **74**. The 2/*m* (C_{2h}) symmetry of **74** (μ-2,5-Me_2pyz) site requires that 2,5-Me_2pyz moieties is disordered; their methyl groups and aromatic H atoms are assigned occupancies of 1/2. Nearly all substituted pyrazines exhibit a lower affinity for **74** than the parent ligand. This trend is predicted from steric effects associated with bulky guest molecules. No spectroscopic evidence was found for the binding of these highly substituted derivatives.

Table 7
Binding constants for **74** with amines

Amine	K/M^{-1}
Dabco	220
Pyrazine (pyz)	56
2-Mepyz	2.8
2,3-Me_2pyz	0.26
2,5-Me_2pyz	0.83
2,3-Et_2pyz	<0.2
2-NH_2pyz	93
2-CH_3Opyz	0.3
2-Clpyz	0.3
Quinoxaline	0.7
Pyridine (py)	0.56
2-Mepy	<0.2
4-Mepy	0.5
3,5-Me_2py	0.6
2-NH_2py	1.0
4-Me_2Npy	2.6

Data collected from ref. [70b].

4. Concluding remarks

This review documents the significant progress made in the area of metallosupramolecular rectangles over the past few years. The rich and varied possibilities for creating rectangles constructed in a step-wise reaction or self-assembly process are described. As a strategy for the synthesis of molecular rectangles, coordination-driven self-assembly proved to be superior to conventional routes, which typically lead to kinetically distributed product formation. Thus, structurally well-defined molecular rectangles can be obtained in high selectivity and quantitative yield under mild conditions through metal-mediated self-assembly. The incorporation of transition metal centers into rectangular-like structures introduces new functionalities, such as luminescence, redox and other properties. The excited state energies of rectangles can be tuned by the judicious choice of ligands and metal centers. The efficiency of luminescence of molecular rectangles can be enormously improved through the incorporation of ligands with extended π-conjugation. An alternate way to improve luminescence properties is the introduction of long alkyl chains in the ligand resulting in aggregation that induces luminescence enhancement. With the improvement in photoluminescent properties and cavity size of these host molecules to external guest, it is possible to use such systems as effective sensors. Thus the design of a class of luminescent and redox-active rectangles, possessing a well-defined cavity size that exhibit new features, will be a worthwhile subject for the further construction of sophisticated models such as artificial photosynthesis, molecular electronics, etc.

Acknowledgements

We gratefully acknowledge the financial support from Academia Sinica, and National Science Council, Taiwan.

References

[1] (a) J.M. Lehn, Angew. Chem. Int. Ed. Engl. 27 (1988) 90;
(b) H.J. Schneider, Angew. Chem. Int. Ed. Engl. 30 (1991) 1417;
(c) B. Olenyuk, A. Fechtenkotter, P.J. Stang, J. Chem. Soc., Dalton Trans. (1998) 1707;
(d) D.L. Caulder, K.N. Raymond, J. Chem. Soc., Dalton Trans. (1999) 1185.

[2] (a) D.J. Braga, J. Chem. Soc., Dalton Trans. (2000) 3705;
(b) H. Li, M. Eddaoudi, M. O'Keeffe, O.M. Yaghi, Nature 402 (1999) 276;
(c) M.J. Zaworotko, Angew. Chem. Int. Ed. 37 (1998) 1211.

[3] (a) P.J. Giordano, M.S. Wrighton, J. Am. Chem. Soc. 101 (1979) 2888;
(b) G.L. Geoffroy, M.S. Wrighton, Organometallic Photochemistry, Academic Press, New York, 1979.

[4] (a) D.J. Stufkens, Comments Inorg. Chem. 13 (1992) 359;
(b) D.J. Stufkens, A. Vleck Jr., Coord. Chem. Rev. 177 (1998) 127.

[5] K. Kalyanasundaram, Photochemistry of Polypyridine and Porphyrin Complexes, Academic Press, London, 1992.

[6] V. Balzani, A. Juris, M. Venturi, S. Campagna, S. Serroni, Chem. Rev. 96 (1996) 759.

[7] K.S. Schanze, D.B. MacQueen, T.A. Perkins, L.A. Cabana, Coord. Chem. Rev. 122 (1993) 63.

[8] K.S. Schanze, K.A. Walters, in: V. Ramamurthy, K.S. Schanze (Eds.), Photoinduced electron transfer in metal-organic dyads, vol. 2, Marcel Dekker, New York, 1998, p. 75.

[9] J.L. Atwood, J.E.D. Davies, D.D. MacNicol, F. Vogtle, J.M. Lehn (Eds.), Comprehensive Supramolecular Chemistry, vols. 6 and 9, Pergamon, Oxford, 1996.

[10] M.J. Blanco, M.C. Jimenez, J.C. Chambron, V. Heitz, M. Linke, J.P. Sauvage, Chem. Soc. Rev. 28 (1999) 293.

[11] (a) A.P. de Silva, H.Q.N. Gunaratne, T. Gunnlaugsson, A.J.M. Huxley, C.P. McCoy, J.T. Rademacher, T.E. Rice, Chem. Rev. 97 (1997) 1515, and references cited therein ;
(b) J.P. Desvergne, A.W. Czarnik (Eds.), Chemosensors of Ion and Molecule Recognition, Kluwer, Boston, 1997.

[12] J.M. Lehn, Supramolecular Chemistry, Concepts and Perspectives, VCH, Weinheim, 1995.

[13] T.D. James, K.R.A.S. Sandanayake, S. Shinkai, Angew. Chem. Int. Ed. Engl. 35 (1996) 1911.

[14] (a) Leininger, B. Olenyuk, P.J. Stang, Chem. Rev. 100 (2000) 853;
(b) M. Fujita, Chem. Soc. Rev. 27 (1998) 417;
(c) C. Kaes, A. Katz, M.W. Hosseini, Chem. Rev. 100 (2000) 3553.

[15] (a) R.V. Slone, J.T. Hupp, C.L. Stern, T.E. Albrecht-schmitt, Inorg. Chem. 35 (1996) 4096;
(b) C.S. Campos-Fernandez, R. Clerac, K.R. Dunbar, Angew. Chem. Int. Ed. 38 (1999) 3477.

[16] (a) J.W. Steed, J.L. Atwood, Supramolecular Chemistry: A Concise Introduction, John Wiley & Sons Ltd., West Sussex, England, 2000;
(b) F.A. Cotton, C. Lin, C.A. Murillo, Acc. Chem. Res. 34 (2001) 759.

[17] (a) B.J. Holliday, C.A. Mirkin, Angew. Chem. Int. Ed. 40 (2001) 2022;
(b) D.L. Caulder, K.N. Raymond, Acc. Chem. Res. 32 (1999) 975;
(c) R.V. Slone, K.D. Benkstein, S. Belanger, J.T. Hupp, I.A. Guzei, A.L. Rheingold, Coord. Chem. Rev. 171 (1998) 221;
(d) S.S. Sun, A.J. Lees, Coord. Chem. Rev. 230 (2002) 171;
(e) F. Würthner, C.C. You, C.R. Saha-Möller, Chem. Soc. Rev. 33 (2004) 133.

[18] (a) M. Eddaoudi, J. Kim, J.B. Wachter, H.K. Chae, M. O'Keeffe, O.M. Yaghi, J. Am. Chem. Soc. 123 (2001) 4368;
(b) M. Schweiger, S.R. Seidel, M. Schmitz, P.J. Stang, Org. Lett. 2 (2000) 1255;
(c) D.K. Chand, K. Biradha, M. Fujita, S. Sakamoto, K. Yamaguchi, Chem. Commun. (2002) 2486;
(d) G.F. Swiegers, T.J. Malefetse, Chem. Rev. 100 (2000) 3483.

[19] K.D. Benkstein, J.T. Hupp, C.L. Stern, J. Am. Chem. Soc. 120 (1998) 12982.

[20] K.D. Benkstein, J.T. Hupp, C.L. Stern, Angew. Chem. Int. Ed. 39 (2000) 2891.

[21] K.D. Benkstein, C.L. Stern, K.E. Splan, R.C. Johnson, K.A. Walters, F.W.M. Vanhelmont, J.T. Hupp, Eur. J. Inorg. Chem. (2002) 2818.

[22] K.E. Splan, A.M. Massari, G.A. Morris, S.S. Sun, E. Reina, S.T. Nguyen, J.T. Hupp, Eur. J. Inorg. Chem. (2003) 2348.

[23] (a) T. Rajendran, B. Manimaran, R.T. Liao, R.J. Lin, P. Thanasekaran, Y.H. Liu, I.J. Chang, S. Rajagopal, K.L. Lu, Inorg. Chem. 42 (2003) 6388;
(b) T. Rajendran, B. Manimaran, F.Y. Lee, G.H. Lee, S.M. Peng, C.M. Wang, K.L. Lu, Inorg. Chem. 39 (2000) 2016.

[24] B. Manimaran, P. Thanasekaran, T. Rajendran, R.T. Liao, Y.H. Liu, G.H. Lee, S.M. Peng, S. Rajagopal, K.L. Lu, Inorg. Chem. 42 (2003) 4795.

[25] H. Hartmann, S. Berger, R. Winter, J. Fiedler, W. Kaim, Inorg. Chem. 39 (2000) 4977.

[26] (a) L. Wallace, D.P. Rillema, Inorg. Chem. 32 (1993) 3836;
(b) J.R. Shaw, R.H. Schmehl, J. Am. Chem. Soc. 113 (1991) 389.

[27] (a) L. Sacksteder, M. Lee, J.N. Demas, B.A. DeGraff, J. Am. Chem. Soc. 115 (1993) 8230;
(b) A.P. Zipp, L. Sacksteder, J. Streich, A. Cook, J.N. Demas, B.A. DeGraff, Inorg. Chem. 32 (1993) 5629.

[28] (a) P. Spellane, R.J. Watts, Inorg. Chem. 32 (1993) 5633;
(b) L. Sacksteder, A.P. Zipp, E.A. Brown, J. Streich, J.N. Demas, B.A. DeGraff, Inorg. Chem. 29 (1990) 4335.

[29] (a) G. Musie, J.H. Reibenspies, M.Y. Darensbourg, Inorg. Chem. 37 (1998) 302;
(b) D.C. Goodman, P.J. Farmer, M.Y. Darensbourg, J.H. Reibenspies, Inorg. Chem. 35 (1996) 4989.

[30] T. Rajendran, B. Manimaran, R.T Liao, Y.H. Liu, P. Thanasekaran, R.J. Lin, I.J. Chang, S. Rajagopal, K.L. Lu, in preparation.

[31] M. Canepa, M.A. Fox, J.K. Whitesell, J. Org. Chem. 66 (2001) 3886.

[32] (a) E. Prasad, K.R. Gopidas, J. Am. Chem. Soc. 122 (2000) 3191;
(b) M.A. Smitha, E. Prasad, K.R. Gopidas, J. Am. Chem. Soc. 123 (2001) 1159;
(c) J.R. Lakowicz, Principles of Fluorescence Spectroscopy, second ed., Kluwer Academic/Plenum Publishers, New York, 1999.

[33] C.L. Kuehl, S.D. Huang, P.J. Stang, J. Am. Chem. Soc. 123 (2001) 9634.

[34] W. Kaim, B. Schwederski, A. Dogan, J. Fiedler, C.J. Kuehl, P.J. Stang, Inorg. Chem. 41 (2002) 4025.

[35] M.J.E. Resendiz, J.C. Noveron, H. Disteldorf, S. Fischer, P.J. Stang, Org. Lett. 6 (2004) 651.

[36] M.S. Luth, E. Freisinger, F. Glahe, J. Muller, B. Lippert, Inorg. Chem. 37 (1998) 3195.

[37] B. Beck, A. Schneider, E. Freisinger, D. Holthenrich, A. Erxleben, A. Albinati, E. Zangrando, L. Randaccio, B. Lippert, Dalton Trans. (2003) 2533.

[38] D. Drew, J.R. Doyle, Inorg. Synth. 28 (1990) 346.

[39] E. Lindner, R. Zong, K. Eichele, U. Weisser, M. Strobele, Eur. J. Inorg. Chem. (2003) 705.

[40] R.D. Sommer, A.L. Rheingold, A.J. Goshe, B. Bosnich, J. Am. Chem. Soc. 123 (2001) 3940.

[41] D.A. Beauchamp, S.J. Loeb, Chem. Commun. (2002) 2484.

[42] O.S. Jung, Y.J. Kim, Y.A. Lee, S.W. Kang, S.N. Choi, Cryst. Growth Des. 4 (2004) 23.

[43] D.P.L. Caradoc-Davies, L.R. Hanton, Dalton Trans. (2003) 1754.
[44] C.Y. Su, Y.P. Cai, C.L. Chen, M.D. Smith, W. Kaim, H.C. zur Loye, J. Am. Chem. Soc. 125 (2003) 8595.
[45] I.B. Rother, M. Willermann, B. Lippert, Supramol. Chem. 14 (2002) 189.
[46] J. Keegan, P.E. Kruger, M. Nieuwenhuyzen, N. Martin, Cryst. Growth Des. 2 (2002) 329.
[47] (a) K.C. Nicolaou, A.L. Smith, in: P.J. Stang, F. Diederich (Eds.), Modern Acetylene Chemistry, VCH, Weinheim, 1995, p. 203;
(b) K.K. Wang, Chem. Rev. 96 (1996) 207.
[48] (a) T.P. Lockhart, P.B. Comita, R.G. Bergman, J. Am. Chem. Soc. 103 (1981) 4082;
(b) R.G. Bergman, Acc. Chem. Res. 6 (1973) 25.
[49] T. Kawano, J. Kuwana, I. Ueda, Inorg. Chem. 41 (2002) 4078.
[50] T. Kawano, J. Kuwana, I. Ueda, Bull. Chem. Soc. Jpn. 76 (2003) 789.
[51] P.L. Caradoc-Davies, D.H. Gregory, L.R. Hanton, J.M. Turnbull, J. Chem. Soc., Dalton Trans. (2002) 1574.
[52] R. Bilewicz, A. Wieckowska, B. Korybut-Daszkiewicz, A. Olszewska, N. Feeder, K. Wozniak, J. Phys. Chem. B 104 (2000) 11430.
[53] C.A. Hunter, R.K. Hyde, Angew. Chem. Intl. Ed. Engl. 35 (1996) 1936.
[54] R. Dreos, G. Nardin, L. Randaccio, P. Siega, G. Tauzher, V. Vrdoljak, Inorg. Chem. 40 (2001) 5536.
[55] G.N. Schrauzer, in: R. Parry (Ed.), Inorganic Syntheses, vol. 11, McGraw-Hill, New York, 1968, p. 61.
[56] K.D. Benkstein, J.T. Hupp, C.L. Stern, Inorg. Chem. 37 (1998) 5404.
[57] S.M. Woessner, J.B. Helms, Y. Shen, B.P. Sullivan, Inorg. Chem. 37 (1998) 5406.
[58] B. Manimaran, T. Rajendran, Y.L. Lu, G.H. Lee, S.M. Peng, K.L. Lu, J. Chem. Soc., Dalton Trans. (2001) 515.
[59] B. Manimaran, P. Thanasekaran, T. Rajendran, R.J. Lin, I.J. Chang, G.H. Lee, S.M. Peng, S. Rajagopal, K.L. Lu, Inorg. Chem. 41 (2002) 5323.
[60] B.Z. Tang, Y. Geng, J.W.Y. Lam, B. Li, X. Jing, X. Wang, F. Wang, A. Pakhomov, X.X. Zhang, Chem. Mater. 11 (1999) 1581.
[61] J. Luo, Z. Xie, J.W.Y. Lam, L. Cheng, H. Chen, C. Qiu, H.S. Kwok, X. Zhan, Y. Liu, D. Zhu, B.Z. Tang, Chem. Commun. (2001) 1740.
[62] (a) C.A. Bunton, F. Nome, F.H. Quina, L.S. Romsted, Acc. Chem. Res. 24 (1991) 357;
(b) M. Gratzel, K. Kalyanasundaram (Eds.), Kinetics and Catalysis in Microheterogeneous Systems, Marcel Dekker, New York, 1991.
[63] J.R. Farrell, A.H. Eisenberg, C.A. Mirkin, I.A. Guzei, L.M. Liable-Sands, C.D. Incarvito, A.L. Rheingold, C.L. Stern, Organometallics 18 (1999) 4856.
[64] A.H. Eisenberg, F.M. Dixon, C.A. Mirkin, C.L. Stern, C.D. Incarvito, A.L. Rheingold, Organometallics 20 (2001) 2052.
[65] F.M. Dixon, A.H. Eisenberg, J.R. Farell, C.A. Mirkin, L.M.L. Sands, A.L. Rheingold, Inorg. Chem. 39 (2000) 3432.
[66] H. Suzuki, N. Tajima, K. Tatsumi, Y. Yamamoto, Chem. Commun. (2000) 1801.
[67] (a) N. Das, P.S. Mukherjee, A.M. Arif, P.J. Stang, J. Am. Chem. Soc. 125 (2003) 13950;
(b) P.S. Mukherjee, N. Das, Y.K. Kryschenko, A.M. Arif, P.J. Stang, J. Am. Chem. Soc. 126 (2004) 2464.
[68] (a) D. Visinescu, M. Andruh, A. Muller, M. Schmidtmann, Y. Journaux, Inorg. Chem. Commun. 5 (2002) 42;
(b) D. Visinescu, G.I. Pascu, M. Andruh, J. Magull, H.W. Roesky, Inorg. Chim. Acta 340 (2002) 201;
(c) D. Visinescu, A.M. Madalan, V. Kravtsov, Y.A. Simonov, M. Schmidtmann, A. Muller, M. Andruh, Polyhedron 22 (2003) 1385.
[69] H. Cheng, D.C. Ying, F.C. Jie, L.Y. Jiang, M.Q. Jin, J. Chem. Soc., Dalton Trans. (2000) 1207.
[70] (a) W. Maverick, F.E. Klavetter, Inorg. Chem. 23 (1984) 4129;
(b) W. Maverick, M.L. Ivie, J.H. Waggenspack, F.R. Fronczek, Inorg. Chem. 29 (1990) 2403.
[71] J.R. Bradbury, J.L. Hampton, D.P. Martone, A.W. Maverick, Inorg. Chem. 28 (1989) 2392.
[72] S.W. Lai, M.G.B. Drew, P.D. Beer, J. Organomet. Chem. 637–639 (2001) 89.
[73] L.M. Field, P.M. Lahti, Inorg. Chem. 42 (2003) 7447.
[74] C. Rancurel, D.B. Leznoff, J.P. Sutter, S. Golhen, L. Ouahab, J. Kliava, O. Kahn, Inorg. Chem. 38 (1999) 4753.
[75] T.J. Boyle, M.A. Rodriguez, T.M. Alam, Dalton Trans. (2003) 4598.
[76] A.K. Duhme, Z. Anorg. Allg. Chem. 624 (1998) 1922.
[77] H. Yan, G.S. Fink, A. Neels, H.S. Evans, J. Chem. Soc., Dalton Trans. (1997) 4345.